2018-03

Higher-order boundary and rough surface treatment of the MMPE model in the evaluation of scattering effects

Tan, Yi Ling; Leigh, Gonzalo H. Veran

Monterey, California: Naval Postgraduate School

NAVAL POSTGRADUATE SCHOOL

MONTEREY, CALIFORNIA

THESIS

HIGHER-ORDER BOUNDARY AND ROUGH SURFACE TREATMENT OF THE MMPE MODEL IN THE EVALUATION OF SCATTERING EFFECTS

by

Yi Ling Tan
Gonzalo H. Veran Leigh

March 2018

Thesis Advisor: Kevin B Smith
Second Reader: Clyde Scandrett

Approved for public release. Distribution is unlimited.

THIS PAGE INTENTIONALLY LEFT BLANK

REPORT DOCUMENTATION PAGE			*Form Approved OMB No. 0704-0188*
Public reporting burden for this collection of information is estimated to average 1 hour per response, including the time for reviewing instruction, searching existing data sources, gathering and maintaining the data needed, and completing and reviewing the collection of information. Send comments regarding this burden estimate or any other aspect of this collection of information, including suggestions for reducing this burden, to Washington headquarters Services, Directorate for Information Operations and Reports, 1215 Jefferson Davis Highway, Suite 1204, Arlington, VA 22202-4302, and to the Office of Management and Budget, Paperwork Reduction Project (0704-0188) Washington DC 20503.			
1. AGENCY USE ONLY ***(Leave blank)***	**2. REPORT DATE** March 2018	**3. REPORT TYPE AND DATES COVERED** Master's thesis	
4. TITLE AND SUBTITLE HIGHER-ORDER BOUNDARY AND ROUGH SURFACE TREATMENT OF THE MMPE MODEL IN THE EVALUATION OF SCATTERING EFFECTS			**5. FUNDING NUMBERS**
6. AUTHOR(S) Yi Ling Tan and Gonzalo H. Veran Leigh			
7. PERFORMING ORGANIZATION NAME(S) AND ADDRESS(ES) Naval Postgraduate School Monterey, CA 93943-5000			**8. PERFORMING ORGANIZATION REPORT NUMBER**
9. SPONSORING /MONITORING AGENCY NAME(S) AND ADDRESS(ES) N/A			**10. SPONSORING / MONITORING AGENCY REPORT NUMBER**
11. SUPPLEMENTARY NOTES The views expressed in this thesis are those of the author and do not reflect the official policy or position of the Department of Defense or the U.S. Government. IRB number ____N/A____.			
12a. DISTRIBUTION / AVAILABILITY STATEMENT Approved for public release. Distribution is unlimited.			**12b. DISTRIBUTION CODE**

13. ABSTRACT (maximum 200 words)

This research aims to improve the Monterey-Miami Parabolic Equation model (MMPE) by incorporating a higher-order hybrid boundary treatment and Fred D. Tappert's field transformational model to add surface scattering to the existing models. The impact of these two additions is investigated for improvements in accuracy and stability to the current MMPE model under rough surface conditions. Both models were treated with a Pierson-Moskowitz rough surface spectrum.

It was hoped that the hybrid model would provide a reduction of the phase errors inherent to the MMPE at long range; however, no improvements were seen, and the sensitivity to depth mesh size was not reduced. This could be the result of errors in the derivation of the higher-order algorithm.

The transformational model used Tappert's field transformation to incorporate surface scattering and is thought to perform better when compared with the hybrid model by capturing higher modes of propagation.

The inclusion of rough surface scattering in both models was evaluated for energy transmission across the air/water interface and beam dispersion. It was observed that the rough surface had minimal impact on energy transmission.

14. SUBJECT TERMS Acoustic propagation, rough sea surface scattering, acoustic scattering, split-step Fourier algorithm, finite difference algorithm			**15. NUMBER OF PAGES** 65
			16. PRICE CODE
17. SECURITY CLASSIFICATION OF REPORT Unclassified	**18. SECURITY CLASSIFICATION OF THIS PAGE** Unclassified	**19. SECURITY CLASSIFICATION OF ABSTRACT** Unclassified	**20. LIMITATION OF ABSTRACT** UU

NSN 7540-01-280-5500 Standard Form 298 (Rev. 2-89)
Prescribed by ANSI Std. 239-18

THIS PAGE INTENTIONALLY LEFT BLANK

Approved for public release. Distribution is unlimited.

HIGHER-ORDER BOUNDARY AND ROUGH SURFACE TREATMENT OF THE MMPE MODEL IN THE EVALUATION OF SCATTERING EFFECTS

Yi Ling Tan
Civilian, Singaporean Defense Science and Technology Agency
National University of Singapore, 2011

Gonzalo H. Veran Leigh
Lieutenant Junior Grade, Peruvian Navy
B.S., Escuela Naval del Peru, 2012

Submitted in partial fulfillment of the
requirements for the degree of

MASTER OF SCIENCE IN ENGINEERING ACOUSTICS

from the

NAVAL POSTGRADUATE SCHOOL
March 2018

Approved by: Kevin B. Smith
Thesis Advisor

Clyde Scandrett
Second Reader

Daphne Kapolka
Chair, Department of Engineering Acoustics

THIS PAGE INTENTIONALLY LEFT BLANK

ABSTRACT

This research aims to improve the Monterey-Miami Parabolic Equation model (MMPE) by incorporating a higher-order hybrid boundary treatment and Fred D. Tappert's field transformational model to add surface scattering to the existing models. The impact of these two additions is investigated for improvements in accuracy and stability to the current MMPE model under rough surface conditions. Both models were treated with a Pierson-Moskowitz rough surface spectrum.

It was hoped that the hybrid model would provide a reduction of the phase errors inherent to the MMPE at long range; however, no improvements were seen, and the sensitivity to depth mesh size was not reduced. This could be the result of errors in the derivation of the higher-order algorithm.

The transformational model used Tappert's field transformation to incorporate surface scattering and is thought to perform better when compared with the hybrid model by capturing higher modes of propagation.

The inclusion of rough surface scattering in both models was evaluated for energy transmission across the air/water interface and beam dispersion. It was observed that the rough surface had minimal impact on energy transmission.

THIS PAGE INTENTIONALLY LEFT BLANK

TABLE OF CONTENTS

THIS PAGE INTENTIONALLY LEFT BLANK

LIST OF FIGURES

THIS PAGE INTENTIONALLY LEFT BLANK

LIST OF TABLES

THIS PAGE INTENTIONALLY LEFT BLANK

LIST OF ACRONYMS AND ABBREVIATIONS

2D	Two-Dimensional
COMSOL	Simulation Model
FD	Finite Difference
FE	Finite Element
MMPE	Monterey Miami Parabolic Equation
PE	Parabolic Equation
PM	Pierson-Moskowitz
SSF	Split-Step Fourier
SSP	Sound Speed Profile
TC-WAPE	Thomson-Chapman Wide Angle Parabolic Equation
UMPE	University of Miami Parabolic Equation

THIS PAGE INTENTIONALLY LEFT BLANK

ACKNOWLEDGMENTS

We would like to express our gratitude to Professor Kevin Smith, our thesis advisor and the creator of MMPE algorithm, for giving us the opportunity and guidance to contribute to the advancement of the MMPE software. We would also like to thank him for furthering our professional development in the acoustics arena by supporting our involvement in the 2017 Acoustical Society of America conference in New Orleans. Above all, Professor Smith has been a kind friend and patient mentor, who gave flexibility and space for us to work confidently. We would also like to thank Professor Clyde Scandrett, who despite his busy schedule as the dean, accommodated our tight schedule for thesis submission and put in much time and effort into correcting our equations.

I would like to thank Professor Daphne Kapolka, whose dedication to acoustics and warm heart for helping students has inspired me. I would also like to thank Professors Bruce Denardo and Oleg Godin, for the many classes I attended that strengthened my fundamentals in acoustics. My sincere gratitude to my then director Chen Yeang Tat and current department head Kelvin Lin from Defense Science and Technology Agency in Singapore, who encouraged my studies, without which this degree would not have happened. Finally, yet importantly, I would like to thank my parents for their persistence in providing me with a good education, which has led me to where I am today, and my husband for his unwavering emotional support that gave me strength to do everything else.

—Yi Ling Tan

I would like to thank the USW program faculty, including teachers from the departments of Physics, Math, Operations Research, Oceanography, Mechanical Engineering and Electrical and Computer Engineering. They have provided support and patience during the past 24 months of countless study and research

hours. I also would like to thank all the instructors of the 2014 class of the Peruvian Submarine School and the 2015 officers and crewmembers of the BAP “Antofagasta” for introducing me to the world of undersea warfare operations and underwater acoustics. Finally, to my parents and brothers, I am grateful for the support and nourishing love during all the times I have been away from home.

—Gonzalo H. Veran Leigh

I. INTRODUCTION

In the evaluation of sonar, an accurate and robust underwater propagation prediction is required to understand system performance. However, it is difficult to accurately and robustly model the underwater environment due to the complexities in replicating the many unknown factors and their interactions, which affect underwater acoustics. Among the different propagation models, the Parabolic Equation model (PE) has been favored for its fast-computational speed and relative accuracy. The Monterey-Miami Parabolic Equation (MMPE) model is a specific PE algorithm created by Professor Kevin Smith in 1999 and has since then undergone several iterations to improve the model's accuracy and robustness. In this thesis, an attempt was made to improve the MMPE model by incorporating a higher-order boundary treatment to its hybrid variant to achieve better accuracy. A higher-order boundary algorithm provides a more accurate modeling of interface density discontinuities with a five-point centered approach compared to the conventional three.

The impact of a higher-order approach was evaluated for accuracy improvements and robustness. Rough surface modeling and scattering effects are also added to emulate a more realistic underwater environment. A Pierson-Moskowitz rough surface spectrum (Pierson & Moskowitz, 1964) was used with Tappert's field transformation (Tappert & Nghiem-Phu, 1985) to incorporate surface scattering on both the hybrid and conventional MMPE model. The revised MMPE model was tested in two simulation scenarios—the shallow and deep waters. In the shallow water scenario modeled after the South China Sea, surface scattering effects on underwater propagation was evaluated for spatial coherence using the hybrid and transformational MMPE model. In the deep-water scenario modeled after the Pacific Ocean, surface scattering effects on energy transmission across the water-air interface was evaluated using only the hybrid MMPE model.

THIS PAGE INTENTIONALLY LEFT BLANK

II. BACKGROUND

Underwater acoustic propagation models based on the parabolic equation (PE) have been commonly developed due to their computational efficiency. Traditionally, some of the numerical methods used are based on finite difference (FD) algorithms while others on finite element (FE) techniques. In 1973, Hardin and Tappert (1973) introduced the split-step Fourier (SSF) algorithm that improved many of the numerical sensitivities associated with FD and FE algorithms.

In 1993, the University of Miami Parabolic Equation (UMPE) research model was developed by Professor Fred Tappert (Smith & Tappert, 1993), which serves as the base model for the Monterey Miami Parabolic Equation (MMPE) model (Smith, 2001). The MMPE is an acoustic propagation model written by Prof. Kevin B. Smith of the Naval Postgraduate School in the mid-1990s. It relies on most of the UMPE model but uses the centered-step scheme in the split-step Fourier algorithm for improved accuracy and efficiency (Ead, 2004). MMPE is written in the Fortran language.

The basic description of the ocean environment consists of depth and range-dependent sound speed profiles in the water column, a range-dependent bottom bathymetry and a range-independent description of the bottom acoustic properties (sound speed, density, sound speed gradient, attenuation, shear speed, and shear attenuation) (K. Smith, class notes, October 26, 2017). There is also a range-dependent sub-bottom bathymetry and associated sub-bottom acoustic properties to emulate a sediment layer over a harder sub-bottom. The source parameters consist of the source depth, source frequency, frequency bandwidth and number of frequency bins. The source is modeled as a point source in the absence of a defined array length; otherwise, the source is modeled as a continuous vertical line array.

A. ORIGINAL MONTEREY MIAMI PARABOLIC EQUATION APPROACH (MMPE)

The original MMPE approach is based on the parabolic equation split-step Fourier algorithm (PE/SSF) (Hardin & Tappert, 1973), with the propagation operator adopting the Thomson-Chapman Wide Angle Parabolic Equation (TC-WAPE) approximation (Thompson & Chapman, 1983). The PE/SSF algorithm treats the surface as an ideal pressure release boundary (perfect reflector) which is automatically satisfied through the SSF algorithm, while the bottom boundary is treated with density smoothing functions to represent the discontinuity in sound speed and density.

Starting with the wave equation in 2D cylindrical coordinates for acoustic pressure $p(r,z)$

$$\frac{1}{r}\frac{\partial}{\partial r}\left(r\frac{\partial p}{\partial r}\right)+\rho\frac{\partial}{\partial z}\left(\frac{1}{\rho}\frac{\partial p}{\partial z}\right)+k_0^2 n^2 p=0 \tag{1}$$

where $n(r,z)=\frac{c_0}{c(r,z)}$ is the acoustic index of refraction, $k_0=\frac{\omega}{c_0}$ is a reference acoustic wavenumber (based on a defined reference sound speed c_0), and $\rho=\rho(z)$ is the medium density as a function of depth (Yevick & Thomson, 1994). By introducing the PE field function defined as

$$\psi(r,z)=\sqrt{k_0 r}\,p(r,z)e^{-ik_0 r} \tag{2}$$

the 2D wave equation can be shown to reduce to a PE of the form

$$\frac{\partial\psi}{\partial r}=-ik_0(1-Q)\psi \tag{3}$$

where the PE propagation operator *Q* is defined as

$$Q=\sqrt{n^2+\frac{\rho}{k_0^2}\frac{\partial}{\partial z}\left(\frac{1}{\rho}\frac{\partial}{\partial z}\right)}. \tag{4}$$

In the original MMPE approach, the PE field function is replaced by the substitution

$$\psi=\sqrt{\rho}\psi \tag{5}$$

which satisfies a PE of the form

$$\frac{\partial \psi}{\partial r} = -ik_0(1-Q)\psi \,. \tag{6}$$

In this case, however, where the PE differential operator is

$$Q = \sqrt{N^2 + \frac{1}{k_0^2}\frac{\partial^2}{\partial z^2}} \tag{7}$$

and where the effective index of refraction is defined by

$$N^2 = n^2 + \frac{1}{2k_0^2}\left[\frac{1}{\rho}\frac{\partial^2 \rho}{\partial z^2} - \frac{3}{2}\left(\frac{1}{\rho}\frac{\partial \rho}{\partial z}\right)^2\right]. \tag{8}$$

The MMPE model uses the TC-WAPE approximation for the PE propagation operator based on the operator splitting

$$Q = \sqrt{1+\varepsilon'+\mu} \approx \sqrt{1+\mu} + \sqrt{1+\varepsilon'} - 1 \tag{9}$$

where

$$\varepsilon' = N^2 - 1 \tag{10}$$

$$\mu = \frac{1}{k_0^2}\frac{\partial^2}{\partial z^2}\,. \tag{11}$$

Formally, one can solve the first order differential equation, assuming no radial difference in the operator Q as a forward marching approximation given by (Hardin & Tappert, 1973).

$$\psi(r+\Delta r, z) \approx \exp\left[-ik_0\Delta r\left(1-Q\right)\right]\psi(r,z)\,. \tag{12}$$

Expanding the propagation operator using the approximated differential operator gives

$$\exp\left[-ik_0\Delta r\left(1-Q\right)\right] \approx \exp\left[-ik_0\Delta r\left(1-\sqrt{1+\mu}\right)\right]\exp\left[-ik_0\Delta r\left(1-\sqrt{1+\varepsilon'}\right)\right]. \tag{13}$$

The SSF algorithm was introduced to efficiently treat this form of operator splitting by noting that the differential operator can be written as a simple scalar operator in the vertical wavenumber domain. Specifically, MMPE utilizes the "centered step" scheme

$$\psi\left(r+\Delta r,z\right)=e^{-ik_0\frac{\Delta r}{2}U_{op}\left(r+\Delta r,z\right)}\times IFFT\left\{e^{-ik_0\Delta r\hat{T}_{op}\left(k_z\right)}\times FFT\left[e^{-ik_0\frac{\Delta r}{2}U_{op}\left(r,z\right)}\times\psi\left(r,z\right)\right]\right\} \quad (14)$$

where

$$T_{op}\left(\frac{\partial^2}{\partial z^2}\right)=1-\sqrt{1+\mu}=1-\sqrt{1+\frac{1}{k_0^2}\frac{\partial^2}{\partial z^2}}\quad\Rightarrow\quad\hat{T}_{op}\left(k_z\right)=1-\sqrt{1-\frac{k_z^2}{k_0^2}} \quad (15)$$

and

$$U_{op}\left(r,z\right)=1-\sqrt{1+\varepsilon'}=1-N=1-n^2-\frac{1}{2k_0^2}\left[\frac{1}{\rho}\frac{\partial^2\rho}{\partial z^2}-\frac{3}{2}\left(\frac{1}{\rho}\frac{\partial\rho}{\partial z}\right)^2\right]. \quad (16)$$

Note that since there are derivatives of ρ in the equation, any step discontinuities in the density profile are smoothed appropriately from ρ_1 to ρ_2 at the depth of the bottom interface $z=z_b$ according to

$$\rho\left(z\right)=\rho_1+\frac{1}{2}\left(\rho_2-\rho_1\right)\left[1+\tanh\left(\frac{z-z_b}{L}\right)\right] \quad (17)$$

where L denotes the transition region of density change.

B. HYBRID SPLIT-STEP FINITE-DIFFERENCE ALGORITHM FOR BOTTOM BOUNDARY TREATMENT

The original Monterey Miami Parabolic Equation (MMPE) treatment of density discontinuity is known to introduce phase errors at long range (Smith, 2001). A hybrid Split Step Fourier (SSF) with Finite Difference (FD) PE approach can reduce these phase errors by splitting the propagation operator into density-independent and density-dependent terms and computing only the density-dependent term with the FD algorithm, while retaining the SSF algorithm for density-independent terms (Yevick & Thomson, 1997). This hybrid approach retains the computational efficiency of the SSF algorithm while enhancing the accuracy of the FD bottom boundary treatment without the use of the density smoothing function.

The hybrid MMPE approach separates the density dependent terms by defining the PE propagation operator in the form:

$$Q = \sqrt{1+\varepsilon+u+\gamma} \tag{18}$$

where

$$\varepsilon = n^2 - 1 \tag{19}$$

$$\mu = \frac{1}{k_0^2}\frac{\partial^2}{\partial z^2} \tag{20}$$

$$\gamma = -\frac{1}{k_0^2 \rho}\frac{\partial \rho}{\partial z}\frac{\partial}{\partial z}. \tag{21}$$

As before, the TC-WAPE approximation is applied to the PE propagation operator as

$$Q = \sqrt{1+\varepsilon+u+\gamma} \approx \sqrt{1+u} + \sqrt{1+\varepsilon} + \sqrt{1+\gamma} - 2. \tag{22}$$

Expansion of the exponential propagation operator now separates the density dependent term from the others as

$$\exp\left[ik_0\Delta r\left(Q-1\right)\right] \approx$$
$$\exp\left[ik_0\Delta r\left(\sqrt{1+\gamma}-1\right)\right]\exp\left[ik_0\Delta r\left(\sqrt{1+u}-1\right)\right]\exp\left[ik_0\Delta r\left(\sqrt{1+\varepsilon}-1\right)\right]. \tag{23}$$

The μ and ε terms are computed as before, using the SSF approach to give the intermediate solution

$$\psi\left(r+\Delta r', z\right) \approx$$
$$IFFT\left\{\exp\left[ik_0\Delta r\left(\sqrt{1+u}-1\right)\right] FFT\left[\exp\left[ik_0\Delta r\left(\sqrt{1+\varepsilon}-1\right)\right]\psi\left(r+\Delta r, z\right)\right]\right\}. \tag{24}$$

The final solution at the end of the range step is then achieved by applying the density-dependent term as

$$\psi\left(r+\Delta r, z\right) \approx \exp\left[ik_0\Delta r\left(\sqrt{1+\gamma}-1\right)\right]\psi\left(r+\Delta r', z\right). \tag{25}$$

The FD approach to the density-dependent term uses the Padé [1,1] approximation (Yevick & Thompson, 1997).

$$\exp\left[ik_0\Delta r\left(\sqrt{1+\gamma}-1\right)\right]\approx\frac{1+\frac{1}{4}\left(1+ik_0\Delta r\right)\gamma}{1+\frac{1}{4}\left(1-ik_0\Delta r\right)\gamma} \tag{26}$$

resulting in

$$\psi\left(r+\Delta r,z\right)\approx\frac{1+\frac{1}{4}\left(1+ik_0\Delta r\right)\gamma}{1+\frac{1}{4}\left(1-ik_0\Delta r\right)\gamma}\psi\left(r+\Delta r',z\right) \tag{27}$$

or

$$\left[1+\frac{1}{4}\left(1-ik_0\Delta r\right)\gamma\right]\psi\left(r+\Delta r,z\right)\approx\left[1+\frac{1}{4}\left(1+ik_0\Delta r\right)\gamma\right]\psi\left(r+\Delta r',z\right). \tag{28}$$

This form can then be treated using implicit finite difference techniques.

Invoking a standard finite different approximation of the operator $\gamma=-\frac{1}{k_0^2\rho}\frac{\partial\rho}{\partial z}\frac{\partial}{\partial z}$ to the field function at a point z_0 results in the 3-point scheme defined by (Yevick & Thomson, 1997)

$$\gamma\psi_0\approx\frac{1}{k_0^2\Delta z^2}\left[\left(\rho_- -1\right)\psi_{-1}-\left(\rho_+ +\rho_- -2\right)\psi_0+\left(\rho_+ -1\right)\psi_{+1}\right] \tag{29}$$

where

$$\psi_0=\psi\left(z_0\right) \tag{30}$$

$$\psi_{-1}=\psi\left(z_0-\Delta z\right) \tag{31}$$

$$\psi_{+1}=\psi\left(z_0+\Delta z\right) \tag{32}$$

$$\rho_{-1}=\rho\left(z_0-\Delta z\right) \tag{33}$$

$$\rho_{+1}=\rho\left(z_0-\Delta z\right) \tag{34}$$

$$\rho_-=\frac{\rho}{\rho_{-0.5}}=\frac{2\rho}{\rho+\rho_{-1}} \tag{35}$$

$$\rho_+=\frac{\rho}{\rho_{+0.5}}=\frac{2\rho}{\rho+\rho_{+1}} \tag{36}$$

$$\rho=\rho\left(z_0\right). \tag{37}$$

This results in the implicit FD expression

$$\alpha(\rho_- - 1)\psi_{-1} + \left[1 - \alpha(\rho_+ + \rho_- - 2)\right]\psi_0 + \alpha(\rho_+ - 1)\psi_{+1} \approx$$
$$\beta(\rho_- - 1)\psi'_{-1} + \left[1 - \beta(\rho_+ + \rho_- - 2)\right]\psi'_0 + \beta(\rho_+ - 1)\psi'_{+1} \quad (38)$$

where

$$\psi = \psi(r + \Delta r, z) \quad (39)$$

$$\psi' = \psi(r + \Delta r', z) \quad (40)$$

$$\alpha = \frac{\frac{1}{4}(1 - ik_0\Delta r)}{k_0^2 \Delta z^2} \quad (41)$$

$$\beta = \frac{\frac{1}{4}(1 + ik_0\Delta r)}{k_0^2 \Delta z^2} \ . \quad (42)$$

The density discontinuity at the bottom interface is defined formally as

$$\rho = \begin{Bmatrix} \rho_w & z < z_b \\ \frac{1}{2}(\rho_w + \rho_b) & for\ z = z_b \\ \rho_b & z > z_b \end{Bmatrix} \quad (43)$$

where ρ_w and ρ_b define the density in the water and bottom, respectively. Near the bottom boundary then, the parameters above reduce to

$$z = z_b - \Delta z, \qquad \rho_- = \frac{2\rho_w}{\rho_w + \rho_w} = 1, \qquad \rho_+ = \frac{4\rho_w}{3\rho_w + \rho_b} \quad (44)$$

$$z = z_b, \qquad \rho_- = \frac{2(\rho_w + \rho_b)}{3\rho_w + \rho_b}, \qquad \rho_+ = \frac{2(\rho_w + \rho_b)}{3\rho_b + \rho_w} \quad (45)$$

$$z = z_b + \Delta z, \qquad \rho_- = \frac{4\rho_b}{3\rho_b + \rho_w}, \qquad \rho_+ = 1. \quad (46)$$

The implicit FD expressions near the boundary then take the forms, from Equation (28).

$$\left[1 + \frac{1}{4}(1 - ik_0\Delta r)\gamma\right]\psi_{zb-1}(r + \Delta r, z) \approx \left[1 - \alpha R_1\right]\psi_{zb-1} + \alpha R_1 \psi_{zb} \quad (47)$$

$$\left[\left[1 + \frac{1}{4}(1 - ik_0\Delta r)\gamma\right]\psi_{zb}(r + \Delta r, z) \approx -\alpha R_1 \psi_{zb-1} + \left[1 - \alpha(R_2 - R_1)\right]\psi_{zb} + \alpha R_2 \psi_{zb+1}\right] \quad (48)$$

$$\left[1+\frac{1}{4}\left(1-ik_0\Delta r\right)\gamma\right]\psi_{zb+1}\left(r+\Delta r,z\right)\approx-\alpha R_2\psi_{zb}+\left[1+\alpha R_2\right]\psi_{zb+1} \tag{49}$$

where

$$R_1=\frac{\rho_w-\rho_b}{3\rho_w+\rho_b} \tag{50}$$

$$R_2=\frac{\rho_w-\rho_b}{3\rho_b+\rho_w}. \tag{51}$$

Then it can be shown that

$$\left[1-\alpha R_1\right]\psi_{zb-1}+\alpha R_1\psi_{zb}\approx\left[1-\beta R_1\right]\tilde{\psi}_{zb-1}+\beta R_1\tilde{\psi}_{zb} \tag{52}$$

$$\begin{aligned}&-\alpha R_1\psi_{zb-1}+\left[1-\alpha\left(R_2-R_1\right)\right]\psi_{zb}+\alpha R_2\psi_{zb+1}\approx\\&-\beta R_1\tilde{\psi}_{zb-1}+\left[1-\beta\left(R_2-R_1\right)\right]\tilde{\psi}_{zb}+\beta R_2\tilde{\psi}_{zb+1}\end{aligned} \tag{53}$$

$$-\alpha R_2\psi_{zb}+\left[1+\alpha R_2\right]\psi_{zb+1}\approx-\beta R_2\tilde{\psi}_{zb}+\left[1+\beta R_2\right]\tilde{\psi}_{zb+1}\,. \tag{54}$$

These three equations with three unknowns can easily be solved algebraically, leading to an efficient solution for the final range step correction in Equation (25).

Although the original MMPE only considered density discontinuities at the water/bottom interface, it is also possible to consider an identical treatment at the water/air interface at the ocean's surface. Such an approach no longer assumes a perfectly reflecting pressure release surface, but directly computes the interaction with a realistic water/air interface. In this case, the density discontinuity at the water/air interface is defined similarly as

$$\rho=\begin{Bmatrix}\rho_a & z<z_s\\ \frac{1}{2}\left(\rho_a+\rho_w\right)\ for\ z=z_s & \\ \rho_w & z>z_s\end{Bmatrix} \tag{55}$$

where z_s refers to the depth of the water/air interface and ρ_a specifies the density of air. In simple cases, this interface depth is defined as $z_s=0$. However, by generalizing the model to treat the water/air boundary discontinuity in a manner similar to the water/bottom interface, the impact of rough surfaces can easily be

accommodated. An equivalent set of algebraic expressions analogous to Equations (49) to (51) can then be defined for the water/air interface.

THIS PAGE INTENTIONALLY LEFT BLANK

III. INVESTIGATION

A. HIGHER-ORDER BOTTOM BOUNDARY TREATMENT

In the previous evaluation of the application of $\gamma = -\frac{1}{k_0^2 \rho}\frac{\partial \rho}{\partial z}\frac{\partial}{\partial z}$ on ψ, a second-order accurate centered finite difference approach was used where

$$\frac{d\psi}{dz} = \psi' \approx \frac{1}{\Delta z}\left[\psi\left(z + \frac{\Delta z}{2}\right) - \psi\left(z - \frac{\Delta z}{2}\right)\right] \tag{55}$$

otherwise represented as

$$\psi' \approx \frac{1}{\Delta z}\left[\psi_{+0.5} - \psi_{-0.5}\right] \tag{56}$$

to improve the accuracy of the first derivative estimation, a fourth-order accuracy approximation is considered, given by

$$\psi' \approx \frac{1}{\Delta z}\left[\psi_{+0.5} - \psi_{-0.5}\right] - \frac{\Delta z^2}{6}\psi''' \tag{57}$$

where

$$\psi''' \approx \frac{1}{\Delta z^3}\left(-\psi_{-1.5} + 3\psi_{-0.5} - 3\psi_{+0.5} + \psi_{+1.5}\right). \tag{58}$$

Substitution of the third-order derivative gives

$$\psi' \approx \frac{1}{\Delta z}\left(\frac{1}{6}\psi_{-1.5} - \frac{3}{2}\psi_{-0.5} + \frac{3}{2}\psi_{+0.5} - \frac{1}{6}\psi_{+1.5}\right). \tag{59}$$

To obtain the second derivative from the first, the approximation

$$\psi'' \approx \frac{1}{\Delta z}\left[\psi'_{+0.5} - \psi'_{-0.5}\right] + \frac{\Delta z^2}{12}\psi'''' \tag{60}$$

is employed, where

$$\psi'''' \approx \frac{1}{\Delta z^4}\left(\psi_{-2} - 4\psi_{-1} + 6\psi_0 - 4\psi_{+1} + \psi_{+2}\right). \tag{61}$$

Substitution of the fourth-order derivative gives

$$\psi'' \approx \frac{1}{\Delta z^2}\left(-\frac{1}{12}\psi_{-2} + \frac{4}{3}\psi_{-1} - \frac{5}{2}\psi_0 + \frac{4}{3}\psi_{+1} - \frac{1}{12}\psi_{+2}\right) \tag{62}$$

$\gamma = -\frac{1}{k_0^2 \rho}\frac{\partial \rho}{\partial z}\frac{\partial}{\partial z}$ can be expressed as a function of $\mu = \frac{1}{k_0^2}\frac{\partial^2}{\partial z^2}$ and its transverse derivative $\tilde{\mu} = \frac{\rho}{k_0^2}\frac{\partial}{\partial z}\left(\frac{1}{\rho}\frac{\partial}{\partial z}\right)$ through the relation $\gamma \equiv \tilde{\mu} - \mu$. Since

$$\mu\psi = \frac{1}{k_0^2}\frac{\partial^2\psi}{\partial z^2} \approx \frac{1}{k_0^2 \Delta z^2}\left(-\frac{1}{12}\psi_{-2} + \frac{4}{3}\psi_{-1} - \frac{5}{2}\psi_0 + \frac{4}{3}\psi_{+1} - \frac{1}{12}\psi_{-2}\right) \tag{63}$$

and

$$\begin{aligned}\tilde{\mu}\psi = \frac{\rho}{k_0^2}\frac{\partial}{\partial z}\left(\frac{1}{\rho}\frac{\partial\psi}{\partial z}\right) \approx \frac{\rho}{k_0^2}\left[\frac{1}{\Delta z}\frac{1}{\rho_{+0.5}}\frac{\partial\psi}{\partial z_{+0.5}} - \frac{1}{\Delta z}\frac{1}{\rho_{-0.5}}\frac{\partial\psi}{\partial z_{-0.5}} + \frac{\Delta z^2}{12\rho}\psi''''\right] \approx \\ \frac{\rho}{k_0^2\Delta z^2}\left[\frac{\Delta z}{\rho_{+0.5}}\left(\frac{\partial\psi}{\partial z_{+0.5}}\right) - \frac{\Delta z}{\rho_{-0.5}}\frac{\partial\psi}{\partial z_{-0.5}} + \frac{1}{12\rho}\left(\psi_{-2} - 4\psi_{-1} + 6\psi_0 - 4\psi_{+1} + \psi_{+2}\right)\right] \approx \\ \frac{\rho}{k_0^2\Delta z^2}\left[\frac{1}{\rho_{+0.5}}\left(\frac{1}{6}\psi_{-1} - \frac{3}{2}\psi_0 + \frac{3}{2}\psi_{+1} - \frac{1}{6}\psi_{+2}\right) - \frac{1}{\rho_{-0.5}}\left(\frac{1}{6}\psi_{-2} - \frac{3}{2}\psi_{-1} + \frac{3}{2}\psi_0 - \frac{1}{6}\psi_{+1}\right)\right. \\ \left. + \frac{1}{12\rho}\left(\psi_{-2} - 4\psi_{-1} + 6\psi_0 - 4\psi_{+1} + \psi_{+2}\right)\right]\end{aligned} \tag{64}$$

then

$$\begin{aligned}\gamma\psi \equiv \left(\tilde{\mu} - \mu\right)\psi \approx \frac{1}{6k_0^2\Delta z^2}\left[\left(1-\rho_-\right)\psi_{-2} + \left(\rho_+ + 9\rho_- - 10\right)\psi_{-1}\right. \\ \left. + \left(18 - 9\rho_+ - 9\rho_-\right)\psi_0 + \left(9\rho_+ + \rho_- - 10\right)\psi_{+1} + \left(1-\rho_+\right)\psi_{+2}\right]\end{aligned} \tag{65}$$

where it was previously defined

$$\rho_- = \frac{\rho}{\rho_{-0.5}} = \frac{2\rho}{\rho + \rho_{-1}} \tag{66}$$

$$\rho_+ = \frac{\rho}{\rho_{+0.5}} = \frac{2\rho}{\rho + \rho_{+1}} \tag{67}$$

$$\rho_{-1} = \rho(z_0 - \Delta z) \tag{68}$$

$$\rho_{+1} = \rho(z_0 - \Delta z). \tag{69}$$

Applying the higher-order FD approximation to the previous marching algorithm

$$\left[1 + \frac{1}{4}\left(1 - ik_0\Delta r\right)\gamma\right]\psi\left(r + \Delta r, z\right) \approx \left[1 + \frac{1}{4}\left(1 + ik_0\Delta r\right)\gamma\right]\psi\left(r + \Delta r', z\right) \tag{70}$$

gives

$$\begin{aligned}
&\alpha_1(1-\rho_-)\psi_{-2}+\alpha_1(\rho_++9\rho_--10)\psi_{-1}+\left[1+\alpha_1(18-9\rho_+-9\rho_-)\right]\psi_0\\
&+\alpha_1(9\rho_++\rho_--10)\psi_{+1}+\alpha_1(1-\rho_+)\psi_{+2}\approx\\
&\beta_1(1-\rho_-)\psi_{-2}+\beta_1(\rho_++9\rho_--10)\psi_{-1}+\left[1+\beta_1(18-9\rho_+-9\rho_-)\right]\psi_0\\
&+\beta_1(9\rho_++\rho_--10)\psi_{+1}+\beta_1(1-\rho_+)\psi_{+2}
\end{aligned}. \qquad (71)$$

Similar to previously defined variables

$$\alpha_1=\frac{\frac{1}{4}(1-ik_0\Delta r)}{6k_0^2\Delta z^2} \qquad (72)$$

$$\beta_1=\frac{\frac{1}{4}(1+ik_0\Delta r)}{6k_0^2\Delta z^2} \qquad (73)$$

Using the same bottom boundary density variations in the MMPE simulations as in the lower-order approach

$$\rho=\begin{cases}\rho_w & z<z_b\\ \frac{1}{2}(\rho_w+\rho_b) & z=z_b.\\ \rho_b & z>z_b\end{cases} \qquad (74)$$

Near the bottom boundary, as in Equations (40) to (42)

$$z=z_b-1,\qquad \rho_-=\frac{2\rho_w}{\rho_w+\rho_w}=1,\qquad \rho_+=\frac{4\rho_w}{3\rho_w+\rho_b} \qquad (75)$$

$$z=z_b,\qquad \rho_-=\frac{2(\rho_w+\rho_b)}{3\rho_w+\rho_b},\qquad \rho_+=\frac{2(\rho_w+\rho_b)}{3\rho_b+\rho_w} \qquad (76)$$

$$z=z_b+1,\qquad \rho_-=\frac{4\rho_b}{3\rho_b+\rho_w},\qquad \rho_+=\frac{2\rho_b}{\rho_b+\rho_b}=1. \qquad (77)$$

Consolidating the three cases yields,

$$\begin{aligned}
&\left[1+\frac{1}{4}(1-ik_0\Delta r)\gamma\right]\psi_{zb-1}(r+\Delta r,z)\approx\\
&\psi_{zb-1}+\alpha_1\left[R_1\psi_{zb-2}-9R_1\psi_{zb-1}+9R_1\psi_{zb}-R_1\psi_{zb+1}\right]
\end{aligned} \qquad (78)$$

$$\left[1+\frac{1}{4}\left(1-ik_0\Delta r\right)\gamma\right]\psi_{zb}\left(r+\Delta r,z\right)\approx$$
$$\psi_{zb}+\alpha_1\left[R_1\psi_{zb-2}+\left(2Q_2+18Q_1-10\right)\psi_{zb-1}+18\left(1-Q_2-Q_1\right)\psi_{zb}\right. \tag{79}$$
$$\left.+\left(18Q_2+2Q_1-10\right)\psi_{zb+1}-R_2\psi_{zb+2}\right]$$

$$\left[1+\frac{1}{4}\left(1-ik_0\Delta r\right)\gamma\right]\psi_{zb+1}\left(r+\Delta r,z\right)\approx$$
$$\psi_{zb+1}+\alpha_1\left[R_2\psi_{zb-1}-9R_2\psi_{zb}+9R_2\psi_{zb+1}-R_2\psi_{zb+2}\right] \tag{80}$$

where

$$R_1=\frac{\rho_w-\rho_b}{3\rho_w+\rho_b} \tag{81}$$

$$R_2=\frac{\rho_w-\rho_b}{3\rho_b+\rho_w} \tag{82}$$

$$Q_1=\frac{\rho_w+\rho_b}{3\rho_w+\rho_b} \tag{83}$$

$$Q_2=\frac{\rho_w+\rho_b}{3\rho_b+\rho_w}. \tag{84}$$

Since

$$\psi_{z_b-2}=\tilde{\psi}_{z_b-2}$$

and

$$\psi_{z_b+2}=\tilde{\psi}_{z_b+2}$$

then

$$\left(1-9\alpha_1R_1\right)\psi_{zb-1}+9\alpha_1R_1\psi_{zb}-\alpha_1R_1\psi_{zb+1}\approx$$
$$\left(\beta_1-\alpha_1\right)R_1\tilde{\psi}_{zb-2}+\left(1-9\beta_1R_1\right)\tilde{\psi}_{zb-1}+9\beta_1R_1\tilde{\psi}_{zb}-\beta_1R_1\tilde{\psi}_{zb+1} \tag{85}$$

$$2\alpha_1\left(Q_2+9Q_1-5\right)\psi_{zb-1}+\left[1+18\alpha_1\left(1-Q_2+Q_1\right)\right]\psi_{zb}+2\alpha_1\left(9Q_2+Q_1-5\right)\psi_{zb+1}\approx$$
$$\left(\beta_1-\alpha_1\right)R_1\tilde{\psi}_{zb-2}+2\beta_1\left(Q_2+9Q_1-5\right)\tilde{\psi}_{zb-1}+\left[1+18\beta_1\left(1-Q_2-Q_1\right)\right]\tilde{\psi}_{zb} \tag{86}$$
$$+2\beta_1\left(9Q_2+Q_1-5\right)\tilde{\psi}_{zb+1}+\left(\alpha_1-\beta_1\right)R_2\tilde{\psi}_{zb+2}$$

$$\alpha_1R_2\psi_{zb-1}-9\alpha_1R_2\psi_{zb}+\left(1+9\alpha_1R_2\right)\psi_{zb+1}\approx$$
$$\beta_1R_2\tilde{\psi}_{zb-1}-9\beta_1R_2\tilde{\psi}_{zb}+\left(1+9\beta_1R_2\right)\tilde{\psi}_{zb+1}+\left(\alpha_1-\beta_1\right)R_2\tilde{\psi}_{zb+2}\ . \tag{87}$$

As before, these three equations with three unknowns can easily be solved algebraically, leading to an efficient solution for the final range step correction in Eq. (25) above. An analogous set of equations is then also defined for the water/air interface.

1. Numerical Results

The higher-order boundary treatment was compared with that of the lower-order method for a flat surface. A “Perkeris” waveguide of 300m depth with an isospeed water column of sound speed 1500m/s overlying a homogeneous sediment half space with geoacoustic properties of sound speed 1800m/s, density 1.8g/cm^3, compressional attenuation of 0.33dB/m/kHz and no shear. A single frequency wide angle source at 100Hz and 180m depth was used and results were compared with validated results generated from the Finite Element (FE) COMSOL model (Littmarck & Saeidi, 2016). Various range and depth mesh sizes were used to compare both programs. It was observed that the hybrid algorithm was highly sensitive to the choice of depth mesh dz. The wrong choice of depth mesh, which deviated from the optimal value, resulted in worse predictions than the non-hybrid algorithm (Smith, Aslan, & Moss, 2017). As seen from Figure 1, the choice of depth mesh other than dz=$\lambda/15$ resulted in large phase errors when we compare the hybrid versus the non-hybrid approach. It was also observed that the higher-order boundary treatment did not perform significantly better or worse than that of the original lower order hybrid approach.

It was discovered that the higher-order equations derived were inaccurate and did not fully capture the higher-order approximations, rendering the solution approximating at second order accuracy as before. This explains why the higher-order equations did not perform any better, but it does not address the possibility that a true fourth order method might.

Derivation of Equations (54) through (84) above were calculated based on differencing schemes provided in the appendix that have subsequently been found to be in error. These errors in turn, resulted in a boundary treatment algorithm that

remains only second order accurate. Specific errors include the "correction term" for Equation (54), which should be divided by 24 instead of 6. This error led to improper formulas given in Equations (59) and (61). An additional error in Equation (61) is due to the fact that instead of the term $\Delta z^2 \psi''' / 12\rho$, the expression $-\Delta z^2 \left(\psi' / \rho\right)''' / 24$ should have been used. In the Appendix, a corrected fourth-order approximation is provided, but there was insufficient time to re-run the simulations. Mathematical alternatives were also discussed in the Appendix and would be of interest to future students to continue to investigate the higher-order approach. Due to the inconclusive nature of the higher-order approach, and the fact that it still has a large sensitivity to depth mesh, the remainder of the results presented use the previously developed second-order accurate finite difference approach to model the effect of density discontinuities for the hybrid MMPE model.

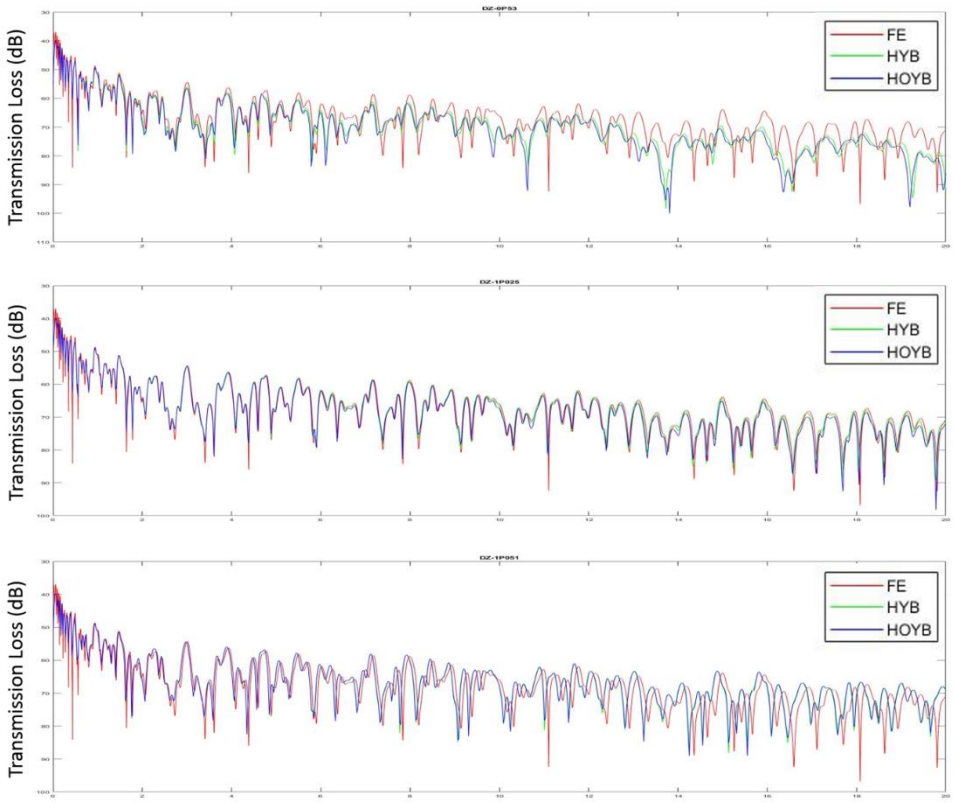

Figure 1. Comparison of higher-order hybrid boundary treatment with lower order boundary treatment against validated FE COMSOL model at z=100m and (upper) dz= $\lambda/30$, (middle) dz= $\lambda/15$ and (lower) dz= $\lambda/10$.

B. ROUGH SURFACE MODELING

Because the hybrid approach to a water/air interface is still being evaluated, it is desired to have an alternative approach to compare against. Preferably, the alternative approach has itself been evaluated as being accurate. However, few models exist that can efficiently generate solutions to rough sea surface scattering. Fortunately, an alternative version of the MMPE model has been previously tested and has demonstrated good performance against both benchmark data and experimental data (Smith, Aslan, & Moss, 2017). This alternative version relies on the Field Transformation Technique (FTT) introduced by Tappert and Nghiem-Phu (1985). A brief overview of that approach is presented here.

1. Rough Surface Scattering with Tappert's Field Transformation

In the evaluation of underwater acoustic propagation, the sea surface is generally treated as a pressure release boundary, while the depth of the sea surface boundary is defined by

$$z = v(r)\,. \tag{88}$$

Here, the physical domain of propagation is bounded by

$$0 \le r \le r_{max} \text{ and } v(r) \le z \le z_{max}.$$

The pressure release boundary condition is defined by

$$\psi\left(z = v(r), r\right) = 0\,. \tag{89}$$

In the evaluation of the image ocean, consider the effect of a sloping surface, where a slope change of $\frac{\partial v}{\partial r}$ introduces a change in angle of the image ray by $2\frac{\partial v}{\partial r}$. A step function in depth is assumed for vertical field symmetry about the pressure release boundary, which satisfies odd symmetry, i.e.

$$\psi\left(-z + 2v(r), r\right) = -\psi(z, r)\,. \tag{90}$$

In contrast the environment (hence, $n\left(z,r\right)$ and U_{op}) satisfies even symmetry

$$U_{op}\left(-z + 2v(r), r\right) = U_{op}\left(z, r\right). \tag{91}$$

this leads to the following set of respective PEs

$$\frac{\partial \psi}{\partial r} = -ik_0\left(T_{op} + U_{op}\right)\psi \quad z > v(r) \text{ Real Ocean} \tag{92}$$

$$\frac{\partial \psi}{\partial r} + 2\frac{\partial v}{\partial r}\frac{\partial \psi}{\partial z} = -ik_0\left(T_{op} + U_{op}\right)\psi \quad z < v(r) \text{ Image Ocean}\,. \tag{93}$$

Tappert and Nghiem-Phu (1985) showed that by defining a field transformation of the form

$$\psi(z,r) = \begin{cases} \psi(z,r) & z > v(r) \text{ Real Ocean} \\ e^{-i2k_0\frac{\partial v}{\partial r}}\psi\left(z, -z + 2v(r)\right) & z < v(r) \text{ Image Ocean} \end{cases} \tag{94}$$

the two respective PEs can be combined into a single PE of the standard form

$$\frac{\partial \tilde{\psi}}{\partial r} = -ik_0\left(T_{op} + \tilde{U}_{op}\right)\tilde{\psi}, \tag{95}$$

where

$$\tilde{U}_{op} = \begin{cases} U_{op}(z,r) & z > v(r) \text{ Real Ocean} \\ U_{op}\left(-z+2v(r),r\right) - 2\dfrac{\partial^2 v}{\partial r^2}(z-v) & z < v(r) \text{ Image Ocean} \end{cases}. \tag{96}$$

This allows the existing SSF approach (using a centered step scheme) to be implemented as

$$\psi\left(r+\Delta r, z\right) = e^{-ik_0\frac{\Delta r}{2}\tilde{U}_{op}(r+\Delta r,z)} \times IFFT\left\{e^{-ik_0\Delta r\tilde{T}_{op}(k_z)} \times FFT\left[e^{-ik_0\frac{\Delta r}{2}\tilde{U}_{op}(r,z)} \times \psi(r,z)\right]\right\} \tag{97}$$

where $\hat{T}_{op}(kz)$ is the same as Equation (15)

$$\hat{T}_{op}(kz) = 1-\sqrt{1+u} = 1-\sqrt{1+\frac{1}{k_0^2}\frac{\partial^2}{\partial z^2}} = 1-\sqrt{1-\frac{k_z^2}{k_0^2}} \tag{98}$$

$$\tilde{U}_{op} = \begin{cases} \hat{U}_{op}(z,r) & z > v(r) \text{ Real Ocean} \\ \hat{U}_{op}\left(-z+2v(r),r\right) - 2\dfrac{\partial^2 v}{\partial r^2}(z-v) & z < v(r) \text{ Image Ocean} \end{cases}. \tag{99}$$

2. Pierson-Moskowitz (PM) Spectrum

The rough surface $v(r)$ is modeled using realizations of a Pierson-Moskowitz (PM) spectrum (see Figure 2). This spectrum assumes that "if the wind blew steadily for a long period over a large sea surface area, the waves would eventually come into equilibrium with the wind". (Pierson & Moskowitz, 1964).

The PM spectrum is empirically found to satisfy the form

$$S_{PM}(\omega) = \frac{\alpha g^2}{\omega^5}\exp\left(-\beta\frac{g^4}{\omega \boldsymbol{U}_{19.5}{}^4}\right) \tag{100}$$

where $\alpha = 8.1\times10^{-3}$ and $\beta = 0.74$ are constants (Pierson & Moskowitz, 1964), $g = 9.8 m/s^2$ is the gravitational constant, and $\boldsymbol{U_{19.5}}$ is the wind speed in m/s at a

height of 19.5m above the sea surface. In terms of angular spatial frequency, where k is in rad/m, the spectrum takes the isotropic form.

$$S_{PM}(k) = \frac{\alpha}{2k^3}\exp\left(-\beta\frac{g^2}{k^2 U_{19.5}{}^4}\right). \tag{101}$$

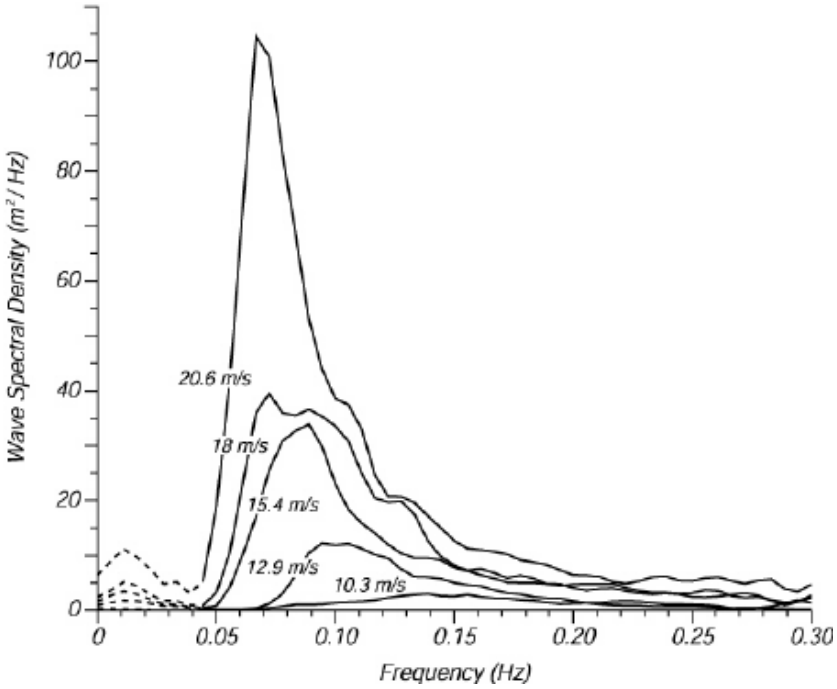

Figure 2. Pierson Moskowitz Spectrum. Source: Pierson & Moskowitz, 1964.

To generate the rough surface realization $v\left(k_r\right)$ from such a defined spectrum, a random realization using a normal distribution is used where $p, \sigma \in N(0,1)$, such that

$$\hat{V}_0(k_r) = \frac{1}{\sqrt{2}}\left[p(k_r) + i\sigma(k_r)\right]\sqrt{\frac{S_{PM}(k_r)}{2}\Delta k} \tag{102}$$

$$\hat{V}(k_r) = \frac{1}{\sqrt{2}}\left[\hat{V}_0(k_r) + \hat{V}_0^*(-k_r)\right] \tag{103}$$

and then

$$v(r) = IFFT\left\{\hat{V}(k_r)\right\}. \tag{104}$$

Referring to Figure 3 below, the validation of the algorithm for generating a surface with the proper PM spectrum was performed by taking sampled points (in red) from the PM spectrum curve and running them through the software that generates rough surface realizations. The resulting surface pattern was transformed back to the spatial frequency domain (in green). The realization surface spectrum was similar to the PM spectrum with small deviations due to the randomization introduced. The MATLAB code that validated the approach to generating properly scaled realizations was then integrated into a version of MMPE for further analysis.

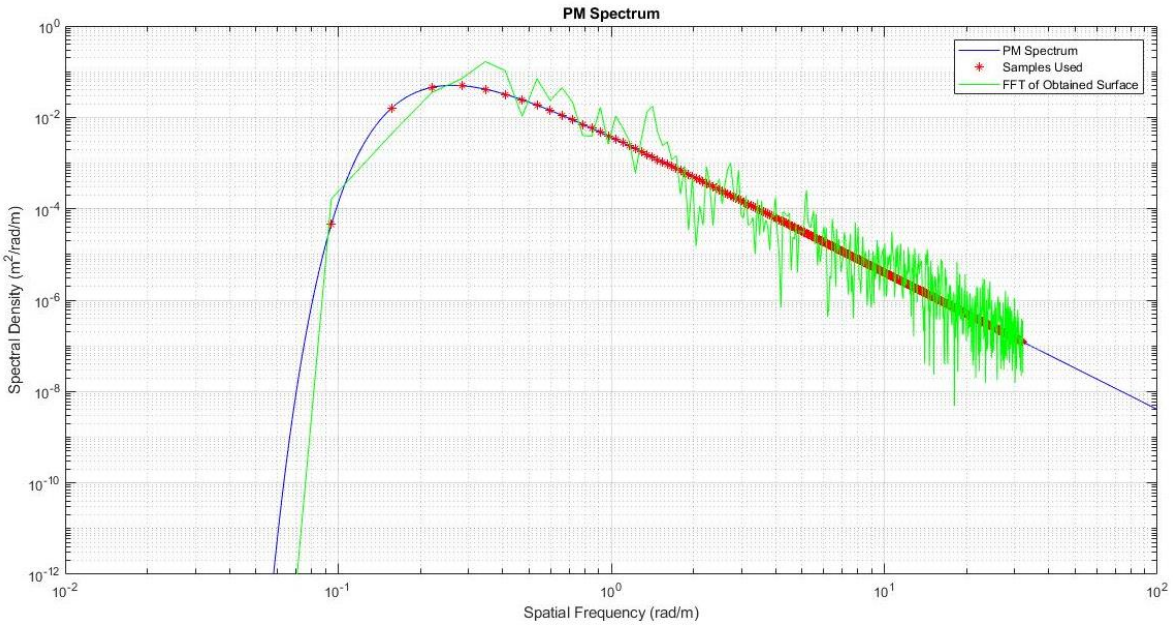

Figure 3. Validation of software for PM spectrum random realization

THIS PAGE INTENTIONALLY LEFT BLANK

IV. SIMULATIONS AND RESULTS

In the subsequent simulations, we compare the field transformational technique approach (Tappert & Nghiem-Phu, 1985), hereafter called the transformational model against the hybrid model (Yevick & Thomson, 1997), hereafter called the hybrid model for the air/water interface utilizing realizations of the Pierson-Moskowitz rough surface spectrum (Pierson & Moskowitz, 1964). It is noted that for both cases, the water-bottom interface uses the Hybrid model.

A. SIMULATION SCENARIO—SHALLOW WATER

In the shallow water scenario, we evaluate the impact of a rough surface scattering on vertical beam width using both the hybrid water/air and FTT pressure release surface MMPE models. We model the environment after that of the South China Sea, where a possible water depth could be 200m, with the following bottom and source parameters shown in Tables 1 and 2 (shear effects are neglected for simplicity):

Table 1. Bottom parameters for shallow water

Depth	200m	
Sound speed profile	Isothermal at 1500m/s	
Surface spectrum	Pierson-Moskowitz spectrum with wind speed of 20m/s	
Bottom properties	Sound speed	1700m/s
	Density	1.5g/cm^3
	Attenuation	0.15dB/km/Hz
Deep bottom properties	Layer depth	30,000m
	Sound speed	1800m/s
	Density	1.8g/cm^3
	Attenuation	0.33dB/km/Hz
Others	Shear effects are neglected in bottom	

Table 2. Source parameters for shallow water:

Source Depth	60m	
Source Frequency	500±300Hz	dz = $\lambda/12$ = 0.250m
	750±300Hz	dz = $\lambda/12$ = 0.167m
	1200±300Hz	dz = $\lambda/10$ = 0.125m

Figure 4 display plots of transmission loss (in dB re 1m) with depth (in m) against range (in km) for the three frequencies (500Hz, 750Hz and 1200Hz) generated using the transformational and hybrid models. Similar propagation structures were observed between the transformational and hybrid models, with the structures becoming more distinct at higher frequencies as expected. The transformational model performed better (primarily due to stability) in all three frequency scenarios and appeared to capture more higher-mode propagation than the hybrid model. The hybrid model showed some degradation, which is more apparent at lower frequencies. Although the hybrid model could potentially provide better accuracy by reducing phase errors at long ranges, it was very depth-mesh sensitive, which contributed to the instability of the hybrid model.

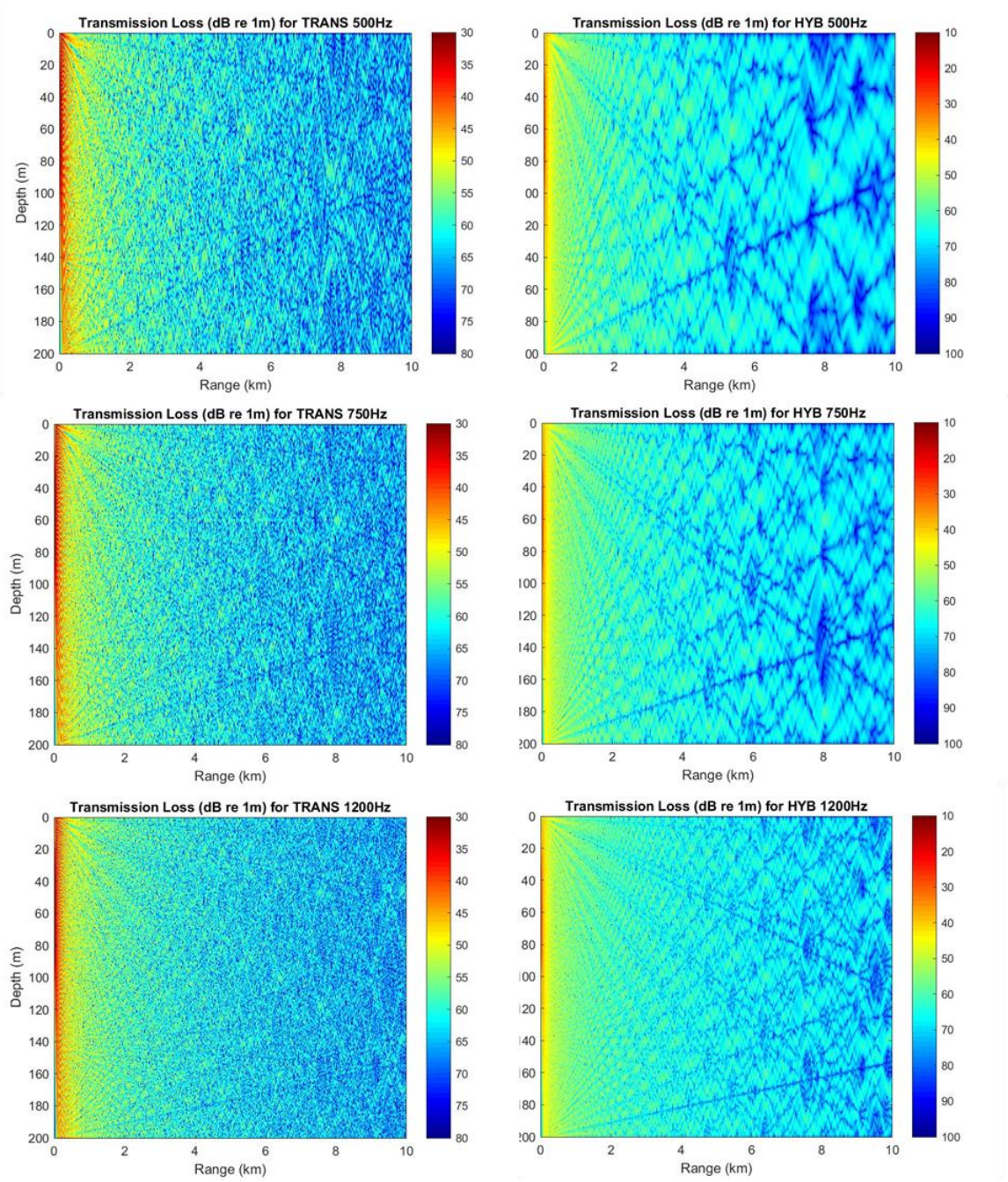

Figure 4. Hybrid versus transformational model

1. Air / Water Energy Transmission

The hybrid model allows us to compute the energy transmission across the air/water interface under various states surface roughness.

In Figure 5, we plot the transmission loss (in dB) against range (in km) measured at a height of two wavelengths above the air/water interface. Three frequencies (500Hz, 750Hz and 1200Hz) were used, and within each frequency, the variation in wind speed and therefore surface roughness does not significantly impact the transmission loss across the interface. This observation was consistent across all frequencies used. With significant scattering, the amount of energy crossing the interface did not change appreciably.

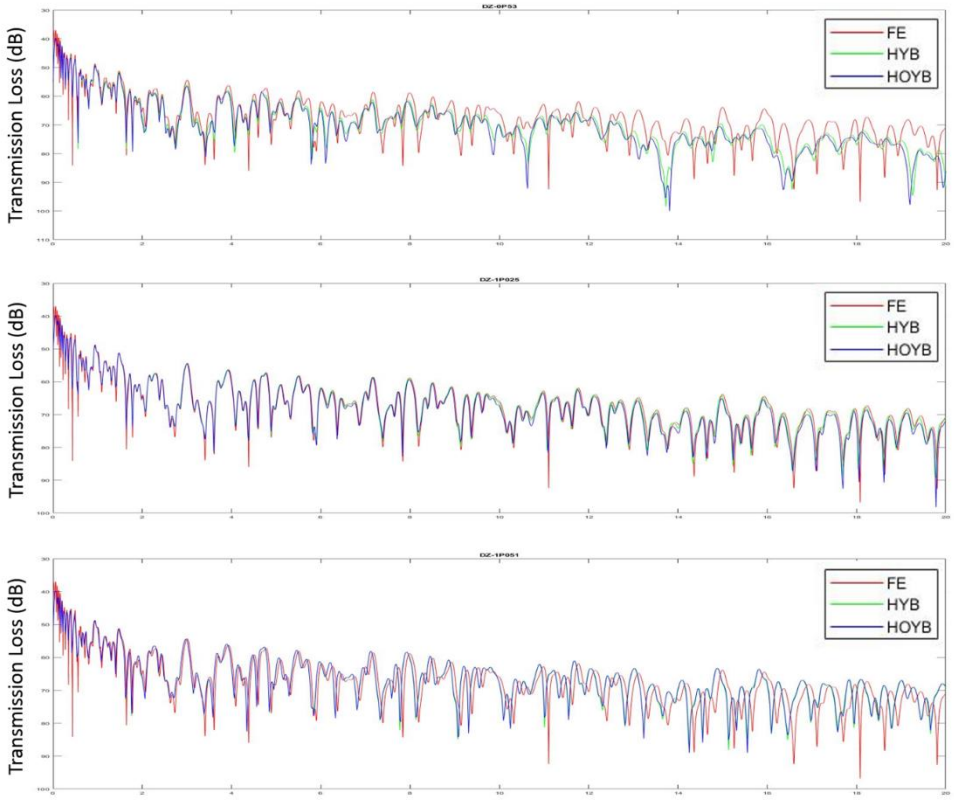

Figure 5. Air/water energy transmission loss versus range, for (upper) 500Hz, (middle) 750Hz and (lower) 1200Hz.

2. Vertical Beam Dispersion at 6km

Next, we investigate the impact that rough surface has on vertical beam dispersion. By extracting all the stored computational data corresponding to the solution in the water column, we synthetically create a linear vertical array that

spans the entire water column of 200m. Source signal was assumed to be impulsive, like with a Hanning window for the coherent source amplitude spectrum.

In Figure 6, we create an arrival time plot for 750Hz and at 5km using wind speeds of 0kts and 25 kits. The arrival time structure is consistent with expectations for a shallow water waveguide. The earliest arrivals correspond to propagation near horizontal (lowest modes) while the later arrivals have undergone multiple boundary reflections from the bottom and surface. It was observed from the arrival time plots that rough surface scattering induced a diffuse spread of energy from surface reflections.

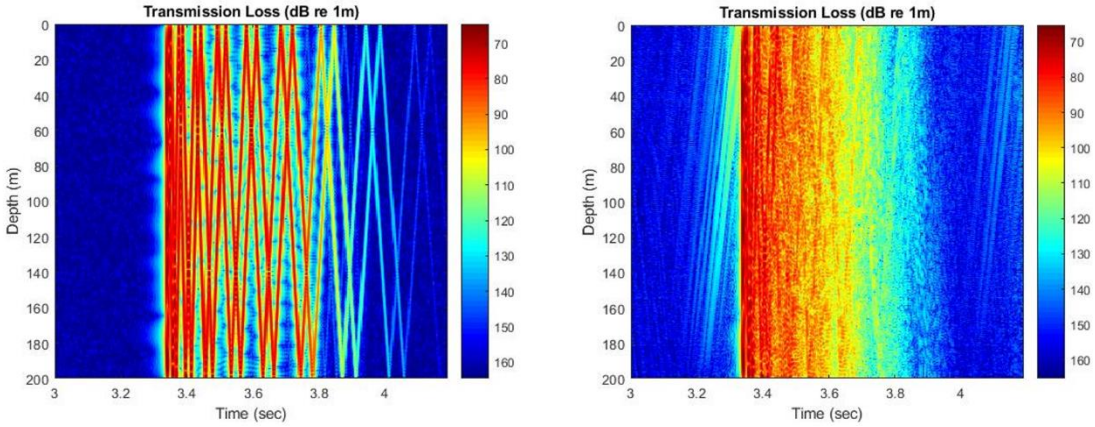

Figure 6. Arrival time structure for 750Hz at 5km for wind speeds (left) 0kts and (right) 25kts

Figure 7 show the arrival angles of one of the ray path from the arrival time plot, computed at 750Hz and at a range of 6km, using the transformational model. The width of such a beam is related to the signal coherence across the array.

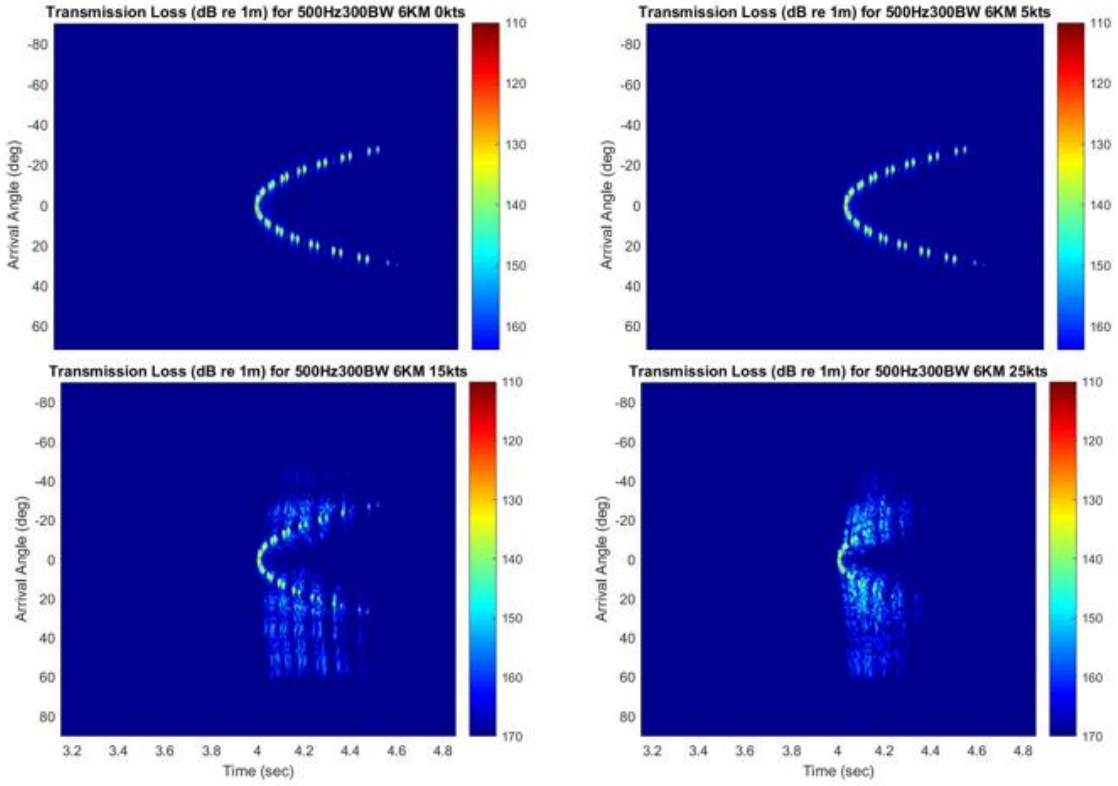

Figure 7. Angles of arrival computed from the transformational model at 6km for the frequency band 500Hz at wind speeds of 0kts, 5kts, 15kts and 25kts

In our analysis, the centers of the virtual arrays were placed at 4km, 6km and 8km from the source. The vertical beam dispersion was evaluated at frequencies of 500Hz, 750Hz and 1200Hz, and at the three ranges mentioned above, under various state of rough surfaces affected by wind speeds of 0kts (flat surface control), 5kts, 15kts and 25kts. Across the parameters used, there are several general observations

- Positive arrival angles correspond to energy propagating downward (from the surface) while negative arrival angles are propagating upward (from the seafloor).
- Both the flat (zero wind) and 5kt wind surfaces produce “clean,” well-defined arrivals in both time and arrival angle. These

correspond to eigenray multipaths between the source and the array downrange.

- By 15kts, the latest arrivals are washed out while nearly all other arrivals show a large spread in arrival angle.
- The positive arrival angles show larger angular spread, dominated by angles greater than the non-scattered field. This suggests that scattering into steeper angles at each surface interaction is much more dominant than forward scatter into more grazing angles.
- The negative arrival angles do not show the same angular extent, since they have undergone an additional bottom bounce. This emphasizes the critical angle cutoff for propagation in this environment.
- As the wind speed increases, there is more scattering near the front of the arrival structure at the lowest angles. More of the later arriving energy has been stripped away from additional surface scattering losses into the bottom.

3. Vertical Beam Width

The use of a 6dB beam widths for arrival angles provided a means for a quantitative analysis of the effects of rough surface scattering on beam dispersion. Figure 8 shows the plot of the 6dB beam width at different ranges of 4km, 6km and 8km and across frequencies of 500Hz, 750Hz and 1200Hz for the transformational and hybrid models. Consistent with the beam dispersion spectra, the 6dB beam width of the arrival angles increased significantly after the 15kts wind speed as observed in the beam dispersion plot. The beam dispersion was more prominent at lower frequencies and the arrival angles tended were larger at higher wind speeds.

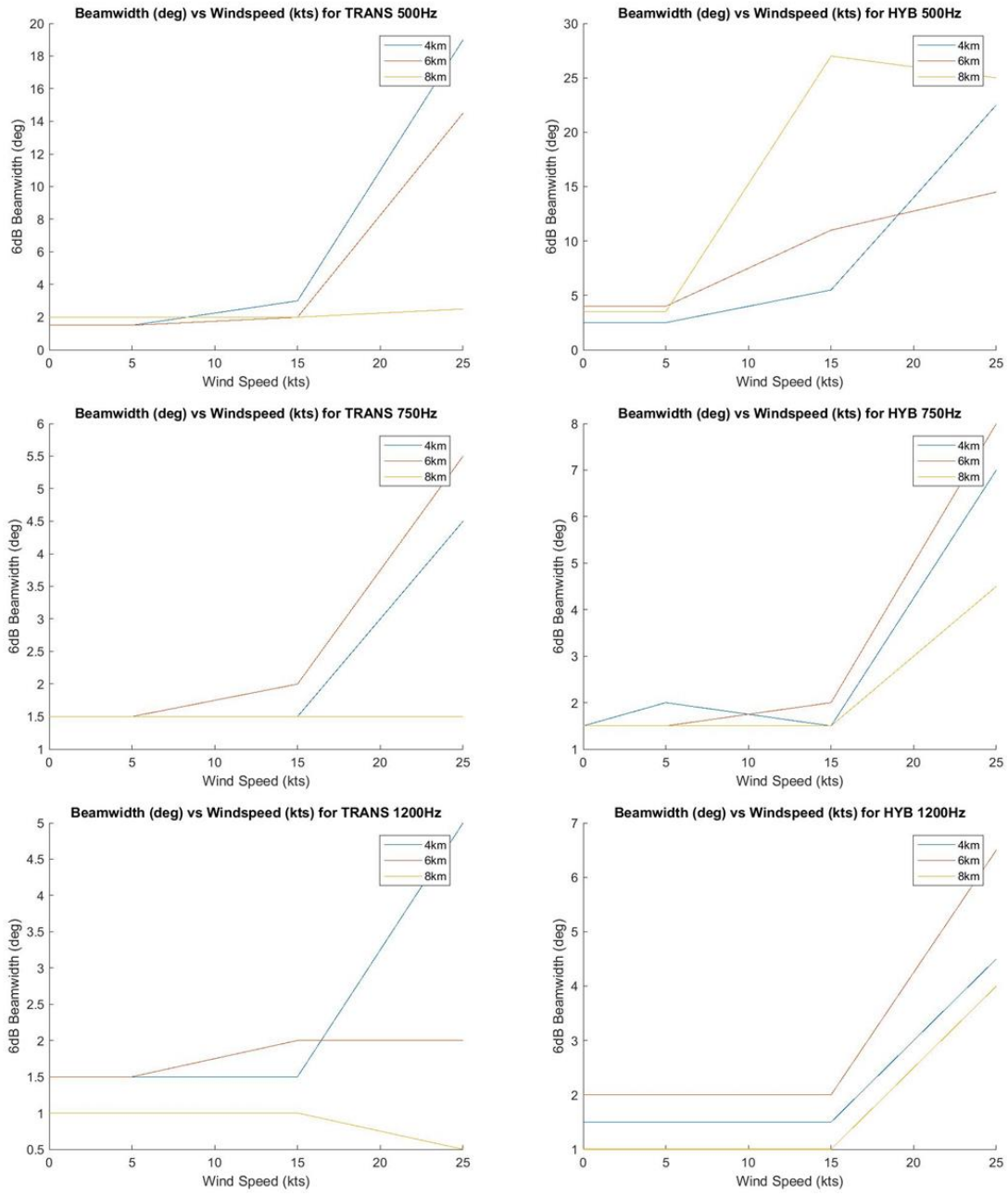

Figure 8. Vertical beam width at 4km, 6km and 8km

B. SIMULATION SCENARIO—DEEP WATER

In the deep-water scenario, we evaluate the effects of rough surface scattering. We used the transformational model and modeled the environment after that of the South Pacific Ocean, where a possible water depth could be

4000m, following a typical Munk's canonical sound speed profile with the following bottom and source parameters shown in Tables 3 and 4 (shear effects are neglected for simplicity):

Table 3. Bottom parameters for deep water

Depth	4000m	
Sound speed profile	Munk's sound speed profile	
Surface spectrum	Pierson-Moskowitz spectrum with wind speed of 25m/s	
Bottom properties	Sound speed	1800m/s
	Density	1.8g/cm^3
	Attenuation	0.25dB/km/Hz
Deep bottom properties	Layer depth	30,000m
	Sound speed	1800m/s
	Density	1.8g/cm^3
	Attenuation	0.33dB/km/Hz
Others	Shear effects are neglected in bottom	

Table 4. Source parameters for deep water

Source depth	60m	
Source frequency	250±50Hz	dz = 0.5m

Computational limitations were encountered in the deep-water scenario, especially at higher frequencies, due to the large FFT size required for generating depth mesh scales small enough to match expected requirements for valid solutions. Only one frequency was tested. Figure 9 below show transmission loss (in dB re 1m) with respect to depth (in m) and range (in km) for a 250Hz source generated using the transformational model for 0,5,15 and 25 knots surface wind speed. It was observed that higher wind speeds registered a slight increase in bottom loss, but it was inconclusive whether the loss was due to computational inaccuracies of the model at the bottom boundary or to the rougher surface.

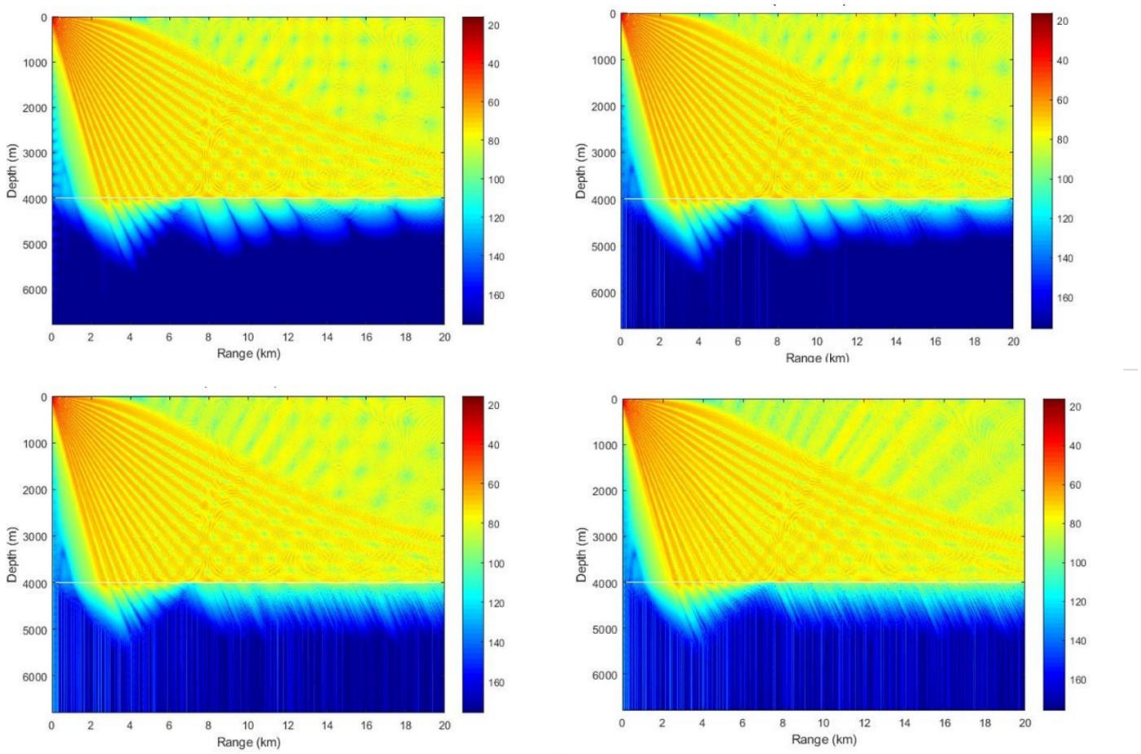

Figure 9. Transmission loss (dB re 1m) for transformational 250Hz at (top left) 0kts, (top right) 5kts, (bottom left) 15kts, (top right) 25kts

As the hybrid model requires more computational space than the transformational model, the model was unable to handle the deep-water scenario leading to an inability to evaluate the energy transmission across the air/water interface. Therefore, deep-water scenario evaluation will remain inconclusive until the program can be improved.

V. CONCLUSIONS

Improvements were made to the MMPE model through the introduction of properly scaled rough surface realizations. Attempts were also made to expand upon the hybrid approach and doing away with the density smoothing approach in favor of a finite difference algorithm, in the hope that the hybrid approach would provide more accurate solutions at long range while maintaining solution stability. We investigated higher-order finite difference approaches for the boundary treatment in the hope of solving the depth-mesh sensitivity issues, but the inherent instability of the hybrid model persisted.

Finally, we investigated impacts of rough surface scattering on propagation in some environment. As expected, we found that rough surface scattering caused arrival angle dispersion, which relates to degraded vertical coherence across the array. Interestingly, this impact was only significant above a threshold wind speed of approximately 15kts. We also discovered that the rough surface scattering has minimal impact on energy transmission across the air/water interface over a wide range of surface roughness. Thus, invoking a pressure release boundary condition remains justified even in the presence of rough surface scattering.

Future work should consider the impact of such rough surface scatter on horizontal coherence across an array at broadside. Formally, this would require a 3D propagation model with a 2D rough surface. Such a version of MMPE is being investigated and could be available for future thesis work.

Due to the instabilities observed with the original hybrid and the higher-order approach attempted here, it may not be worth the relatively minor improvement in long-range phase accuracy to implement the hybrid method in future MMPE versions. While it is important to test the corrected expressions, we noted early in the thesis, it is also important to test the original MMPE smoothing method over the strong water/air interface discontinuity. This approach may still provide a stable, reasonable solution.

THIS PAGE INTENTIONALLY LEFT BLANK

APPENDIX. FINITE DIFFERENCE (FD) APPROXIMATIONS

We will discuss mathematical alternatives for FD approximation. They are based on Taylor's Series Expansion.

A. CURRENT APPROACH

The approximation to the first-order derivative with fourth-order accuracy for $\boldsymbol{\psi}$ was obtained from Taylor's expansion (Stewart, 2015)

$$\psi\left(z+\Delta z\right)=\psi_{+1}=\psi_0+\Delta z\psi_0'+\frac{\left(\Delta z\right)^2}{2!}\psi_0''+\frac{\left(\Delta z\right)^3}{3!}\psi_0^{(3)}+\frac{\left(\Delta z\right)^4}{4!}\psi_0^{(4)} \tag{105}$$

$$\psi\left(z-\Delta z\right)=\psi_{-1}=\psi_0+\Delta z\psi_0'+\frac{\left(\Delta z\right)^2}{2!}\psi_0''-\frac{\left(\Delta z\right)^3}{3!}\psi_0^{(3)}+\frac{\left(\Delta z\right)^4}{4!}\psi_0^{(4)} \tag{106}$$

Where the difference of the two equations gave

$$\psi_0'=\frac{1}{2\Delta z}\left(\psi_{+1}-\psi_{-1}\right)+\frac{\left(\Delta z\right)^2}{3!}\psi_0''' \tag{107}$$

Which could otherwise be represented as follows for half range steps

$$\psi_0'=\frac{1}{\Delta z}\left(\psi_{+0.5}-\psi_{-0.5}\right)+\frac{\left(\Delta z\right)^2}{3!}\psi_0''' \tag{108}$$

The approximation for third derivative with second-order accuracy can be obtained from

$$\psi_0^{(n)}=\frac{\delta_{\Delta z}^n\left[\psi\right]\left(z\right)}{\Delta z^n}=\frac{\sum_{i=0}^{n}\left(-1\right)^i\binom{n}{i}\psi\left(z+\left(\frac{n}{2}-i\right)\Delta z\right)}{\Delta z^n} \tag{109}$$

This equation only gives second-order accuracy for higher derivatives of ψ, which gave

$$\psi'''\approx\frac{1}{\Delta z^3}\left(-\psi_{-1.5}-3\psi_{-0.5}-3\psi_{+0.5}+\psi_{+1.5}\right) \tag{110}$$

Substitution of the third-order derivative gave

$$\psi'\approx\frac{1}{\Delta z}\left(\frac{1}{6}\psi_{-1.5}-\frac{3}{2}\psi_{-0.5}+\frac{3}{2}\psi_{+0.5}-\frac{1}{6}\psi_{+1.5}\right) \tag{111}$$

Similarly, the approximation to the second-order derivative with fourth-order accuracy for ψ was obtained from Taylor's expansion (Stewart, 2015)

$$\psi\left(z+\Delta z\right)=\psi_{+1}=\psi_0+\Delta z\psi_0'+\frac{\left(\Delta z\right)^2}{2!}\psi_0''+\frac{\left(\Delta z\right)^3}{3!}\psi_0'''+\frac{\left(\Delta z\right)^4}{4!}\psi_0\text{''''} \tag{112}$$

$$\psi\left(z-\Delta z\right)=\psi_{-1}=\psi_0-\Delta z\psi_0'+\frac{\left(\Delta z\right)^2}{2!}\psi_0''-\frac{\left(\Delta z\right)^3}{3!}\psi_0'''+\frac{\left(\Delta z\right)^4}{4!}\psi_0\text{''''} \tag{113}$$

where the sum of the two equations gave

$$\psi''\approx\frac{1}{\Delta z^2}\left[\psi_{-1}-2\psi_0-\psi_{+1}\right]-\frac{\Delta z^2}{12}\psi\text{''''} \tag{114}$$

The sample points could also be represented as the difference of first derivatives with second-order accuracy in half range steps

$$\frac{1}{\Delta z}\left[\psi_{+0.5}'-\psi_{-0.5}'\right]=\frac{1}{\Delta z^2}\left[\psi_{-1}-2\psi_0-\psi_{+1}\right] \tag{115}$$

Combining the two equations result in the following with a change in sign of coefficient for ψ''''

$$\psi''\approx\frac{1}{\Delta z}\left[\psi_{+0.5}'-\psi_{-0.5}'\right]+\frac{\Delta z^2}{24}\psi\text{''''} \tag{116}$$

where the fourth derivative with second-order accuracy was obtained from

$$\psi_0^{(n)}=\frac{\delta_{\Delta z}^n\left[\psi\right]\left(z\right)}{\Delta z^n}=\frac{\sum_{i=0}^{n}\left(-1\right)^i\binom{n}{i}\psi\left(z+\left(\frac{n}{2}-i\right)\Delta z\right)}{\Delta z^n} \tag{117}$$

This equation only gives second-order accuracy for higher derivatives of ψ, which gave

$$\psi\text{''''}\approx\frac{1}{\Delta z^4}\left(\psi_{-2}-4\psi_{-1}+6\psi_0-4\psi_{+1}+\psi_{+2}\right) \tag{118}$$

Substitution of the fourth-order derivative gave

$$\psi''\approx\frac{1}{\Delta z^2}\left(-\frac{1}{12}\psi_{-2}+\frac{4}{3}\psi_{-1}-\frac{5}{2}\psi_0+\frac{4}{3}\psi_{+1}-\frac{1}{12}\psi_{+2}\right) \tag{119}$$

This result for the second-order derivative with fourth-order accuracy matched that of known FD coefficients. Consequently, this approach can be used

to obtain the second-order derivative with fourth-order accuracy from that of first-order derivative with fourth-order accuracy in the evaluation of $\gamma = -\frac{1}{k_0^2 \rho}\frac{\partial \rho}{\partial z}\frac{\partial}{\partial z}$ term.

B. HIGHER-ORDER ALTERNATIVE

From the previous case, we can analyze another mathematical alternative to approximate the first-order derivative with fourth-order accuracy. Also obtained from Taylor's expansion (Stewart, 2015)

$$\psi\left(z+\Delta z\right)=\psi_{+1}=\psi_0+\Delta z\psi_0'+\frac{\left(\Delta z\right)^2}{2!}\psi_0''+\frac{\left(\Delta z\right)^3}{3!}\psi_0^{(3)}+\frac{\left(\Delta z\right)^4}{4!}\psi_0^{(4)} \tag{120}$$

$$\psi\left(z-\Delta z\right)=\psi_{-1}=\psi_0+\Delta z\psi_0'+\frac{\left(\Delta z\right)^2}{2!}\psi_0''-\frac{\left(\Delta z\right)^3}{3!}\psi_0^{(3)}+\frac{\left(\Delta z\right)^4}{4!}\psi_0^{(4)} \tag{121}$$

Where the difference of the two equations gave

$$\psi_0'=\frac{1}{2\Delta z}\left(\psi_{+1}-\psi_{-1}\right)-\frac{\left(\Delta z\right)^2}{3!}\psi_0''' \tag{122}$$

Which could otherwise be represented as follows for half range steps

$$\psi_0'=\frac{1}{\Delta z}\left(\psi_{+0.5}-\psi_{-0.5}\right)-\frac{\left(\Delta z\right)^2}{24}\psi_0''' \tag{123}$$

The approximation for third derivative with second-order accuracy can be obtained from

$$\psi_0^{(n)}=\frac{\delta_{\Delta z}^n\left[\psi\right]\left(z\right)}{\Delta z^n}=\frac{\sum_{i=0}^{n}\left(-1\right)^i\binom{n}{i}\psi\left(z+\left(\frac{n}{2}-i\right)\Delta z\right)}{\Delta z^n} \tag{124}$$

This equation only gives second-order accuracy for higher derivatives of ψ, which gave

$$\psi'''\approx\frac{1}{\Delta z^3}\left(-\psi_{-1.5}+3\psi_{-0.5}-3\psi_{+0.5}+\psi_{+1.5}\right) \tag{125}$$

Substitution of the third-order derivative gave

$$\psi'=\frac{1}{8\Delta z}\left(\frac{1}{3}\psi_{-1.5}-9\psi_{-0.5}+9\psi_{+0.5}-\frac{1}{3}\psi_{+1.5}\right)+O\left(\Delta z^4\right) \tag{126}$$

Similarly, the approximation to the second-order derivative with fourth-order accuracy for ψ was obtained from Taylor's expansion (Stewart, 2015)

$$\psi\left(z+\Delta z\right)=\psi_{+1}=\psi_0+\Delta z\psi_0'+\frac{\left(\Delta z\right)^2}{2!}\psi_0''+\frac{\left(\Delta z\right)^3}{3!}\psi_0'''+\frac{\left(\Delta z\right)^4}{4!}\psi_0\text{''''} \tag{127}$$

$$\psi\left(z-\Delta z\right)=\psi_{-1}=\psi_0-\Delta z\psi_0'+\frac{\left(\Delta z\right)^2}{2!}\psi_0''-\frac{\left(\Delta z\right)^3}{3!}\psi_0'''+\frac{\left(\Delta z\right)^4}{4!}\psi_0\text{''''} \tag{128}$$

Where the sum of the two equations gave

$$\psi''\approx\frac{1}{\Delta z^2}\left[\psi_{-1}-2\psi_0+\psi_{+1}\right]-\frac{\Delta z^2}{12}\psi\text{''''} \tag{129}$$

The sample points could also be represented as the difference of first derivatives with second-order accuracy in half range steps

$$\frac{1}{\Delta z}\left[\psi_{+0.5}'-\psi_{-0.5}'\right]=\frac{1}{\Delta z^2}\left[\psi_{-1}-2\psi_0+\psi_{+1}\right] \tag{130}$$

Combining the two equations result in the following with a change in sign of coefficient for ψ''''

$$\psi''\approx\frac{1}{\Delta z}\left[\psi_{+0.5}'-\psi_{-0.5}'\right]-\frac{\Delta z^2}{24}\psi\text{''''} \tag{131}$$

where the fourth derivative with second-order accuracy was obtained from

$$\psi_0^{(n)}=\frac{\delta_{\Delta z}^n\left[\psi\right]\left(z\right)}{\Delta z^n}=\frac{\sum_{i=0}^{n}\left(-1\right)^i\binom{n}{i}\psi\left(z+\left(\frac{n}{2}-i\right)\Delta z\right)}{\Delta z^n} \tag{132}$$

This equation only gives second-order accuracy for higher derivatives of ψ, which gave

$$\psi\text{''''}\approx\frac{1}{\Delta z^4}\left(\psi_{-2}-4\psi_{-1}+6\psi_0-4\psi_{+1}+\psi_{+2}\right) \tag{133}$$

Substitution of the fourth-order derivative gave

$$\psi''\approx\frac{1}{\Delta z^2}\left(-\frac{1}{12}\psi_{-2}+\frac{4}{3}\psi_{-1}-\frac{5}{2}\psi_0+\frac{4}{3}\psi_{+1}-\frac{1}{12}\psi_{+2}\right) \tag{134}$$

In the previous evaluation of the application of $\gamma=-\frac{1}{k_0^2\rho}\frac{\partial\rho}{\partial z}\frac{\partial}{\partial z}$ on ψ, a second-order accurate centered finite difference approach was used where

$$\frac{d\psi}{dz} = \psi' \approx \frac{1}{\Delta z}\left[\psi\left(z + \frac{\Delta z}{2}\right) - \psi\left(z - \frac{\Delta z}{2}\right)\right] \tag{135}$$

otherwise represented as

$$\psi' \approx \frac{1}{\Delta z}\left[\psi_{+0.5} - \psi_{-0.5}\right] \tag{136}$$

To improve the accuracy of the first derivative estimation, a fourth-order accuracy approximation is considered, given by

$$\psi' \approx \frac{1}{\Delta z}\left[\psi_{+0.5} - \psi_{-0.5}\right] - \frac{\Delta z^2}{24}\psi''' \tag{137}$$

where

$$\psi''' \approx \frac{1}{\Delta z^3}\left(-\psi_{-1.5} + 3\psi_{-0.5} - 3\psi_{+0.5} + \psi_{+1.5}\right) \tag{138}$$

Substitution of the third-order derivative gives

$$\psi' \approx \frac{1}{8\Delta z}\left(\frac{1}{3}\psi_{-1.5} - 9\frac{3}{2}\psi_{-0.5} + 9\frac{3}{2}\psi_{+0.5} - \frac{1}{3}\psi_{+1.5}\right) \tag{139}$$

To obtain the second derivative from the first, the approximation

$$\psi'' \approx \frac{1}{\Delta z}\left[\psi'_{+0.5} - \psi'_{-0.5}\right] - \frac{\Delta z^2}{24}\psi'''' \tag{140}$$

Is employed, where

$$\psi'''' \approx \frac{1}{\Delta z^4}\left(\psi_{-2} - 4\psi_{-1} + 6\psi_0 - 4\psi_{+1} + \psi_{+2}\right) \tag{141}$$

Substitution of the fourth-order derivative gives

$$\psi'' \approx \frac{1}{\Delta z^2}\left(-\frac{1}{12}\psi_{-2} + \frac{4}{3}\psi_{-1} - \frac{5}{2}\psi_0 + \frac{4}{3}\psi_{+1} - \frac{1}{12}\psi_{+2}\right) \tag{142}$$

In the evaluation of $= -\frac{1}{k_0^2\rho}\frac{\partial\rho}{\partial z}\frac{\partial}{\partial z}$, the equation made use of $\mu = \frac{1}{k_0^2}\frac{\partial^2}{\partial z^2}$ and its transverse derivative $\tilde{\mu} = \frac{\rho}{k_0^2}\frac{\partial}{\partial z}\left(\frac{1}{\rho}\frac{\partial}{\partial z}\right)$ through the relation $\gamma \equiv \tilde{\mu} - \mu$

$$\mu\psi = \frac{1}{k_0^2}\frac{\partial^2\psi}{\partial z^2} \approx \frac{1}{k_0^2\Delta z^2}\left(-\frac{1}{12}\psi_{-2} + \frac{4}{3}\psi_{-1} - \frac{5}{2}\psi_0 + \frac{4}{3}\psi_{+1} - \frac{1}{12}\psi_{-2}\right) \tag{143}$$

and

$$\beta\psi = \frac{\rho}{k_0^2}\frac{\partial}{\partial z}\left(\frac{1}{\rho}\frac{\partial\psi}{\partial z}\right) \approx$$

$$\frac{4\rho_0}{3\Delta z^2}\left[-\frac{1}{16\rho_{+1}}\psi_{+2} + \frac{1}{\rho_{+0.5}}\psi_{+1} + \left(\frac{1}{16\rho_{+1}} - \frac{1}{\rho_{+0.5}} - \frac{1}{\rho_{-0.5}} + \frac{1}{16\rho_{-1}}\right)\psi_0 + \frac{1}{\rho_{-0.5}}\psi_{-1} - \frac{1}{16\rho_{-1}}\psi_{-2}\right] \tag{144}$$

Then

$$\gamma\psi \equiv (\beta - \mu)\psi \approx \frac{1}{k_0^2\Delta z^2}\left[\left(1 - \frac{\rho_0}{\rho_{-1}}\right)\psi_{-2} - 16\left(1 - \frac{\rho_0}{\rho_{-0.5}}\right)\psi_{-1}\right.$$
$$\left. + \left(\frac{\rho_0}{\rho_{-1}} - 16\frac{\rho_0}{\rho_{-0.5}} - 16\frac{\rho_0}{\rho_{-0.5}} + \frac{\rho_0}{\rho_{-1}} + 30\right)\psi_0 - 16\left(1 - \frac{\rho_0}{\rho_{+0.5}}\right)\psi_{+1} + \frac{1}{12}\left(1 - \frac{\rho_0}{\rho_{+1}}\right)\psi_{+2}\right] + O\left[(\Delta z)^2\right] \tag{145}$$

where it was previously defined that

$$\rho_- = \frac{\rho}{\rho_{-0.5}} = \frac{2\rho}{\rho + \rho_{-1}} \tag{146}$$

$$\rho_+ = \frac{\rho}{\rho_{+0.5}} = \frac{2\rho}{\rho + \rho_{+1}} \tag{147}$$

$$\rho_{-1} = \rho(z_0 - \Delta z) \tag{148}$$

$$\rho_{+1} = \rho(z_0 - \Delta z) \tag{149}$$

$$\rho_{-0.5} = \rho\left(z_0 + \frac{\Delta z}{2}\right) \tag{150}$$

$$\rho_{+1} = \rho\left(z_0 + \frac{\Delta z}{2}\right) \tag{151}$$

Applying the higher-order FD approximation to the previous marching algorithm

$$\left[1 + \frac{1}{4}(1 - ik_0\Delta r)\gamma\right]\psi(r + \Delta r, z) \approx \left[1 + \frac{1}{4}(1 + ik_0\Delta r)\gamma\right]\psi(r + \Delta r', z) \tag{152}$$

gives

$$\alpha_1\left(1-\frac{\rho_0}{\rho_{-1}}\right)\psi_{-2}+16\alpha_1\left(1-\frac{\rho_0}{\rho_{-0.5}}\right)\psi_{-1}+\left[1+\alpha_1\left(\frac{\rho_0}{\rho_1}-16\frac{\rho_0}{\rho_{0.5}}-16\frac{\rho_0}{\rho_{-0.5}}+\frac{\rho_0}{\rho_{-1}}+30\right)\right]\psi_0$$
$$-16\alpha_1\left(1-\frac{\rho_0}{\rho_{0.5}}\right)\psi_1+\alpha_1\left(1-\frac{\rho_0}{\rho_{-1}}\right)\psi_{+2}\approx$$
$$\beta_1\left(1-\frac{\rho_0}{\rho_{-1}}\right)\psi_{-2}-16\beta_1\left(1-\frac{\rho_0}{\rho_{-0.5}}\right)\psi_{-1}+\left[1+\beta_1\left(\frac{\rho_0}{\rho_1}-16\frac{\rho_0}{\rho_{0.5}}-16\frac{\rho_0}{\rho_{-0.5}}+\frac{\rho_0}{\rho_{-1}}+30\right)\right]\psi_0 \quad (153)$$
$$+16\beta_1\left(1-\frac{\rho_0}{\rho_{0.5}}\right)\psi_{+1}+\beta_1\left(1-\frac{\rho_0}{\rho_{-1}}\right)\psi_{+2}$$

where similar to previously defined variables

$$\alpha_1=\frac{(1-ik_0\Delta r)}{48k_0^2\Delta z^2} \quad (154)$$

$$\beta_1=\frac{(1+ik_0\Delta r)}{48k_0^2\Delta z^2} \quad (155)$$

Using the same bottom boundary density variations in the MMPE simulations as per the lower-order approach

$$\rho=\begin{cases}\rho_w & z<z_b\\ \frac{1}{2}(\rho_w+\rho_b) & z=z_b\\ \rho_b & z>z_b\end{cases} \quad (156)$$

Near the bottom boundary, same as (41) to (43)

$$z=z_b-1,\qquad \rho_-=\frac{2\rho_w}{\rho_w+\rho_w}=1,\qquad \rho_+=\frac{4\rho_w}{3\rho_w+\rho_b} \quad (157)$$

$$z=z_b,\qquad \rho_-=\frac{2(\rho_w+\rho_b)}{3\rho_w+\rho_b},\qquad \rho_+=\frac{2(\rho_w+\rho_b)}{3\rho_b+\rho_w} \quad (158)$$

$$z=z_b+1,\qquad \rho_-=\frac{4\rho_b}{3\rho_b+\rho_w},\qquad \rho_+=\frac{2\rho_b}{\rho_b+\rho_b}=1 \quad (159)$$

THIS PAGE INTENTIONALLY LEFT BLANK

LIST OF REFERENCES

Aslan, M., & Smith, K. B. (2017). Modal analysis of split-step Fourier parabolic equation solutions in the presence of rough surface scattering. *The Journal of the Acoustical Society of America, 141(5)*, 3708-3708. doi:10.1121/1.4988106.

Ead, R. (2004). *Predicting the effects of sea surface scatter on broadband pulse propagation with an ocean acoustic parabolic equation* (Master's thesis). Retrieved from https://calhoun.nps.edu/handle/10945/1160

F. D. Tappert & L. Nghiem-Phu. (1985), A new split-step Fourier algorithm for solving the parabolic wave equation with rough surface scattering, *The Journal of the Acoustical Society of America, 77*, S101. doi.org/10.1121/1.2022130

Hardin, R. H. and Tappert, F. D. (1973). *Applications of the split-step Fourier method to the numerical solution of nonlinear and variable coefficient wave equations*, SIAM Rev. 15, 423.

Littmarck, S., Saeidi, F., COMSOL Inc. (Released 2016, Version 5.2) [Multiphysics modeling software]. Retrieved from https://www.comsol.com/.

Pierson, W.J, & Moskowitz, L. (1964) A proposed spectral form for fully developed wind seas based on the similarity theory of S. A. Kitaigorodskii. *Journal of Geophysical Research, 69(24)*. doi:10.1029/JZ069i024p05181

Smith, K., & Tappert, F. (1993). *UMPE: The University of Miami Parabolic Equation Model. Version 1.0*. Retrieved from http://handle.dtic.mil/100.2/ADA270570

Stewart, J. (2015), *Single Variable Calculus: Early Transcendentals 8th edition*. Boston, MA: Cengage Learning.

Tappert, F. (1974). Parabolic equation method in underwater acoustics. *The Journal of the Acoustical Society of America*, 55(S1). doi:10.1121/1.1919661

Thomson, D., & Chapman, N. (1983). A wide-angle split-step algorithm for the parabolic equation. *The Journal of the Acoustical Society of America, 74(6).* doi:10.1121/1.390272

Yevick D., & Thomson, D. J. (1997). A hybrid split-step/finite-difference PE algorithm for variable-density media. *The Journal of the Acoustical Society of America*,*101(3),* 1328-1335. doi:10.1121/1.418160

THIS PAGE INTENTIONALLY LEFT BLANK

INITIAL DISTRIBUTION LIST

1. Defense Technical Information Center
   Ft. Belvoir, Virginia

2. Dudley Knox Library
   Naval Postgraduate School
   Monterey, California